



CRANFIELD UNIVERSITY

**ÓSCAR RODRÍGUEZ FERNÁNDEZ**

**LUNAR MISSION ONE:  
DESCENT & LANDING**

SCHOOL OF AEROSPACE, TRANSPORT AND  
MANUFACTURING

MSc in Astronautics and Space Engineering

Group Design Project  
Academic Year: 2015-2016

Supervisors:  
Dr Jennifer Kingston  
Prof David Cullen  
April 2016



CRANFIELD UNIVERSITY

SCHOOL OF AEROSPACE, TRANSPORT AND  
MANUFACTURING  
MSc in Astronautics and Space Engineering

GROUP DESIGN PROJECT  
Academic Year 2015-16

ÓSCAR RODRÍGUEZ FERNÁNDEZ

Lunar Mission One:  
Descent & Landing

Supervisors:  
Dr Jennifer Kingston  
Prof David Cullen  
April 2016

This thesis is submitted in partial (30%) fulfilment of the requirements for the degree of Master of Science in Astronautics and Space Engineering.

©Cranfield University 2016. All rights reserved. No part of this publication may be reproduced without the written permission of the copyright owner.



# Abstract

As part of a Group Design Project in the MSc in AStronautics and Space Engineering of Cranfield University a design study of Lunar Mission One has been carried. This document contains the work developed in the Descent and Landing Work Package for Lunar Mission One, a crowdfunded robotic mission that aims to drill on the Lunar South Pole in the year 2024.

The objectives of the work presented here is to study and design a landing sequence that allows the spacecraft to land on the desired landing location. In order to do so, the requirements needed to land are derived and analysed here. Several landing guidance logics has been studied and two control algorithms are proposed to conform the descent sequence. This descent sequence is split in three phases: a braking phase, an approach phase and a vertical constant velocity descent. A GNC scheme and sensors for the descent are suggested. Those sensors include optical cameras, lidar instruments and inertial measurement units.

The performance of the proposed solution is assessed by the development of a simulator using MATLAB®. The results show that the proposed solution is able to fulfil all the requirements and a precise landing on the desired location is possible.



# Contents

<b>Contents</b>	<b>iii</b>
<b>List of figures</b>	<b>vii</b>
<b>List of tables</b>	<b>ix</b>
<b>Abbreviations</b>	<b>xi</b>
<b>Symbols</b>	<b>xii</b>
<b>1 Introduction</b>	<b>1</b>
1.1 Overview . . . . .	1
1.2 Descent and Landing Work Package . . . . .	2
1.3 Outline of the thesis organisation . . . . .	3
<b>2 Requirements</b>	<b>4</b>
2.1 Mission Statement . . . . .	4
2.2 Descent and Landing Top-Level Requirements . . . . .	4
2.3 Landing Site Location . . . . .	5
<b>3 Descent Sequence</b>	<b>7</b>
3.1 Introduction . . . . .	7
3.2 Descent Baseline . . . . .	8
3.3 Modelling of the dynamics of the lander . . . . .	9

---

3.4	Descent Strategies . . . . .	11
3.4.1	Direct Collocation Methods . . . . .	12
3.4.2	Gravity turn . . . . .	13
3.4.3	Zero-Effort-Miss/Zero-Velocity-Miss algorithm improved using Model Predictive Static Programming . . . . .	13
3.4.4	Optimal Control Theory . . . . .	16
3.5	Mission scenario for the descent . . . . .	20
<b>4</b>	<b>Hardware for descent and landing</b>	<b>21</b>
4.1	Introduction . . . . .	21
4.2	Main Engine Selection . . . . .	22
4.3	Mapping camera . . . . .	23
4.3.1	Mapping Camera Sizing . . . . .	24
4.4	Guidance Navigation and Control Scheme . . . . .	25
<b>5</b>	<b>Simulation, Analysis and Performance of the Landing</b>	<b>28</b>
5.1	Introduction . . . . .	28
5.2	Simulator Development . . . . .	28
5.2.1	The braking phase model . . . . .	29
5.2.2	Approach Phase . . . . .	31
5.2.3	Vertical Descent . . . . .	33
5.3	The descent and landing simulator . . . . .	33
5.3.1	Plant Dynamics . . . . .	34
5.3.2	Sensors . . . . .	34
5.3.3	Guidance laws . . . . .	34
5.3.4	Attitude Dynamics and Engine Dynamics . . . . .	35
5.3.5	Disturbances . . . . .	35
5.4	Analysis of the results . . . . .	36
5.4.1	Nominal Descent Trajectory . . . . .	36

---

5.4.2	Performance of the algorithms . . . . .	40
<b>6</b>	<b>Conclusions and future work</b>	<b>42</b>
6.1	Conclusions . . . . .	42
6.2	Future Work . . . . .	43
<b>References</b>		<b>44</b>
<b>A</b>	<b>Executive Summary: LMO - Descent &amp; Landing</b>	<b>49</b>
A.1	Requirements . . . . .	49
A.2	Mission Scenario . . . . .	50
A.3	Mapping Camera . . . . .	50
A.4	Hardware for Descent & Landing . . . . .	51
A.5	Descent Sequence . . . . .	52
<b>B</b>	<b>Common Appendix</b>	<b>53</b>
B.1	Mission Statement . . . . .	53
B.2	System Requirements . . . . .	53
B.3	Work Break down Structure . . . . .	56
B.4	Baseline . . . . .	57
B.5	Mission Timeline . . . . .	61
B.5.1	Launch and Early Operations Phase (LEOP) . . . . .	61
B.5.2	Lunar transfer . . . . .	62
B.5.3	Lunar insertion and mapping . . . . .	63
B.5.4	Descent and Landing . . . . .	64
B.5.5	On-surface operations and science . . . . .	65
B.5.6	Overall timeline of Lunar Mission One . . . . .	66
B.6	Budgets . . . . .	67
B.6.1	Cost Budget . . . . .	67
B.6.2	Power Budget . . . . .	68

---

---

B.6.3	$\Delta V$ Budget	69
B.6.4	Communication	70
B.6.5	Data rates	72
B.7	Configuration	73
<b>C</b>	<b>Calculations</b>	<b>77</b>
C.1	Preliminary calculation	77
C.1.1	Soft-Landing	77
C.1.2	Hard-landing	79
C.2	Mapping Camera	81
<b>D</b>	<b>Datasheets</b>	<b>83</b>
D.1	Aerojet R-42DM	83
D.2	Honeywell Miniature IMU	84
D.3	Northrop Grumman LN-200S IMU	85
D.4	Efacec Lidar Velocimeter/Altimeter	87
D.5	DragonEye Flash Lidar 3D Camera	89

# List of Figures

1.1	Work Break Down Structure of the project . . . . .	2
2.1	Location of potential landing sites in the Lunar South Pole [1] . . . . .	6
3.1	Spherical coordinate system used in the equations of motion . . . . .	10
3.2	3D representation of the descent trajectory generated using the Improved ZEM/ZEV with MPSP . . . . .	15
3.3	Coordinate system and angles definition . . . . .	17
4.1	Aerojet R-42DM . . . . .	22
4.2	Proposed GNC scheme for the descent . . . . .	26
5.1	New reference system for the descent . . . . .	32
5.2	Overview of the descent simulator . . . . .	33
5.3	Plant Dynamics . . . . .	34
5.4	Guidance laws . . . . .	35
5.5	Nominal trajectory in topocentric axes for the descent . . . . .	36
5.6	Detail of nominal trajectory in topocentric axes for the descent . . . . .	37
5.7	Nominal altitude profile for the descent . . . . .	37
5.8	Nominal velocity profile for the descent . . . . .	38
5.9	Nominal mass profile for the descent . . . . .	38
5.10	Nominal throttle profile for the descent . . . . .	39
5.11	Summary of the nominal descent sequence . . . . .	40
5.12	Landing ellipse of the mission computed with 1000 simulations . . . . .	41

---

---

A.1	Proposed GNC scheme for the descent . . . . .	51
A.2	Summary of the nominal descent sequence . . . . .	52
B.1	Chart of Work Breakdown Structure . . . . .	56
B.2	Possible landing sites at the South Pole Atkin near Shackleton Crater labelled SR1, SR2 and SR3 [1] . . . . .	57
B.3	CAD representation of the LM1 Lander . . . . .	58
B.4	Fairing Dimensions of the Falcon-9 Full Thrust, Space X (2015) . . .	73
B.5	Spacecraft stowed inside the Falcon-9 Full Thrust fairing . . . . .	74
B.6	Spacecraft top view . . . . .	75
B.7	Spacecraft front view . . . . .	75
B.8	Spacecraft internal view . . . . .	76

# List of Tables

2.1	Potential landing sites on the Lunar South Pole . . . . .	5
3.1	Descent Preliminary Budgets . . . . .	7
3.2	Parameters of the trajectory using the improved ZEM/ZEV algorithm with MPSP . . . . .	15
3.3	Descent Mission Scenario . . . . .	20
4.1	Characteristics of the Aerojet R-42DM . . . . .	22
4.2	Characteristics of the mapping imager . . . . .	24
4.3	Sensor Optics . . . . .	24
4.4	Budget of MARDI camera . . . . .	25
4.5	Budget of the mapping camera . . . . .	25
4.6	Sensors for GNC and Hazard Detection and Avoidance . . . . .	27
5.1	Parameters of the descent phases . . . . .	39
5.2	Budgets for descent and landing . . . . .	39
5.3	Montecarlo Simulation Parameters . . . . .	41
A.1	Mapping Camera Parameters . . . . .	50
A.2	Hardware for Descent and Landing . . . . .	51
A.3	Parameters of the descent phases . . . . .	52
B.1	Components list . . . . .	59
B.2	Drill sub-system components list . . . . .	60

---

---

B.3	Spacecraft sub-system mass . . . . .	60
B.4	Spacecraft landing mass . . . . .	60
B.5	Spacecraft final mass (wet mass) . . . . .	60
B.6	Summary of LEO phase . . . . .	62
B.7	Summary of Lunar Transfer Phase . . . . .	63
B.8	Summary of Lunar insertion and Mapping Phase . . . . .	64
B.9	Summary of Descent and Landing . . . . .	64
B.10	Summary of on-surface operations and science phase . . . . .	65
B.11	Mission timeline summary . . . . .	67
B.12	Table of cost . . . . .	67
B.13	Power consumption throughout the mission . . . . .	68
B.14	Overall Power Consumption . . . . .	68
B.15	Mission $\Delta V$ Budget . . . . .	69
B.16	Spacecraft Antennas technical information . . . . .	70
B.17	Ground Station Details . . . . .	71
B.18	Spacecraft Instrument Data rates . . . . .	72
C.1	Relevant parameters for the soft-landing calculations . . . . .	78
C.2	Orbit and Viewing Calculations for the mapping camera . . . . .	81
C.3	Pixel Parameters and Data Rate . . . . .	81
C.4	Sensor Integration Parameters . . . . .	81
C.5	Sensor Optics . . . . .	82
C.6	Sensor Radiometry . . . . .	82

# Abbreviations

AOCS	Attitude and Orbit Control Subsystem
COTS	Commercial off-the-shelf
FOV	Field of View
GDP	Group Design Project
GNC	Guidance, Navigation and Control
HDA	Hazard Detection and Avoidance
IFOV	Instantaneous Field of View
IMU	Inertial Measurement Unit
LMO	Lunar Mission One
MPSP	Model Predictive Static Programming
STEM	Science, Technology, Engineering and Mathematics
TRL	Technology Readiness Level
WP	Work Package
ZEM	Zero Effort Miss
ZEV	Zero Velocity Miss

# Symbols

$\Delta V$	Delta-v
$m$	Mass
$\mu_M$	Standard Gravitational Parameter of the Moon, $4.9028 \cdot 10^{12} \text{ m}^3 \cdot \text{s}^{-2}$
$R_M$	Radius of the Moon, 1738200 m
$I_{sp}$	Specific Impulse
$r$	Radial distance
$v$	velocity
$g_M$	Gravity on the Moon Surface, $1.62 \text{ m} \cdot \text{s}^{-2}$
$\mathbf{g}$	Gravity vector
$T$	Thrust
$KE$	Kinetic Energy
$t$	Time
$k$	Throttle position, $\in [0, 1]$
$\omega_M$	Mean rotational velocity of the Moon, $2.662 \cdot 10^{-6} \text{ rad} \cdot \text{s}^{-1}$
$\phi, \theta$	Position angles
$\alpha, \beta$	Attitude angles
$H$	Hamiltonian
$\mathbf{p}$	Costates vector
$\mathcal{U}$	Subspace of admissible controls
$D$	Aperture Diameter
a	Acceleration

# Chapter 1

## Introduction

### 1.1 Overview

Lunar Mission One (LMO) is the most inspirational Moon project since the Apollo landings. It is the first crowd funded mission to the Moon [2] and, besides its scientific goals, it has a strong educational element by promoting STEM subjects through its global educational initiative. LMO will send an unmanned robotic spacecraft to the Lunar South Pole by 2024 to perform world-leading science into the origin of the Moon and the planets, drilling to a minimum depth of 20 m and it will create a billion year archive of life on Earth.

The top-level science drivers for Lunar Mission One are [3]:

1. Understand the geochemistry/mineralogy of the lunar crust.
2. Characterize the impact history of the landing site and constrain the age of the South Pole-Aitken Basin.
3. Understand the diversity and origin of lunar polar volatiles.
4. Constraint models of the lunar interior.
5. Characterize the lunar environment for future scientific exploitation and human exploration.
6. Identify resources for future human space exploration.
7. Assess the potential of the lunar surface as a platform for astronomical observations.
8. Science Education.

## 1.2 Descent and Landing Work Package

As part of the LMO's global education and public outreach programme, Cranfield University is providing support to the mission technology through this Group Design Project. The focus of the project is to design the whole mission from the engineering point of view.

This report collects the work developed in the Descent and Landing Work Package, enclosed under the Mission's top-level Work Package as shown in figure 1.1. Due to the nature of the work developed here, close collaboration with the Orbits and the Attitude and Orbit Control Subsystem (AOCS) Work Packages is needed.

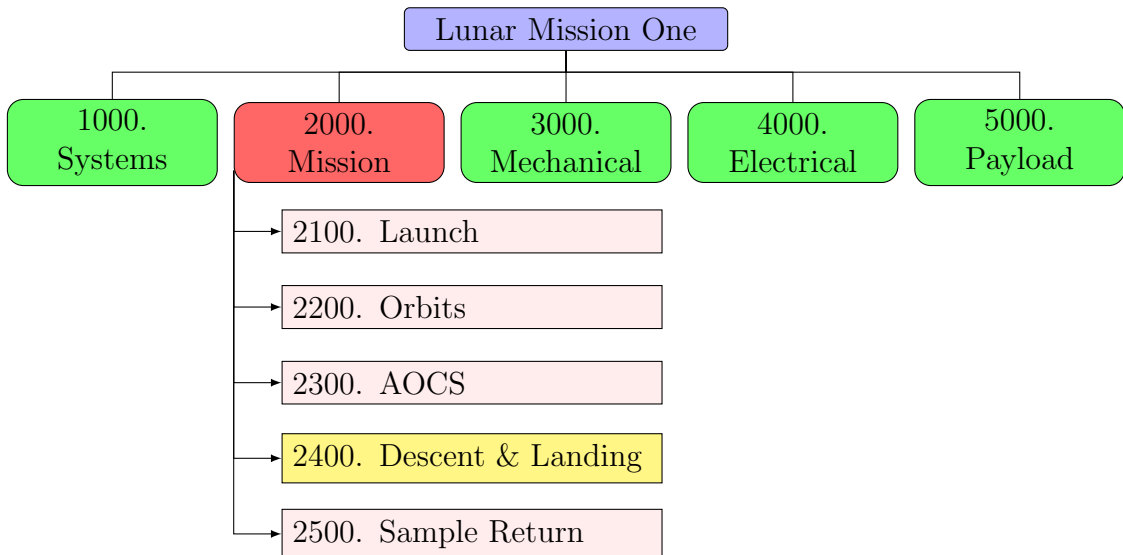


**Figure 1.1:** Work Break Down Structure of the project

The main objective of this WP is to identify, analyse and design all the operations necessary to perform a successful landing in a previously chosen landing location in the Moon's surface. In order to achieve this goal, the main objective has been split into several tasks. These tasks are listed below:

1. Analysis of the landing site location. The landing location will introduce a series of constraints and requirements that will affect the overall mission.
2. Analysis and design of the landing strategy. Focusing on the development of the landing Guidance, Navigation and Control Subsystem (GNC).
3. Analysis, design and/or selection of the hardware needed for landing.

Task 1 will be focused on the analysis of the top level requirements of the mission and in the determination of the derived requirements that will affect not only the Descent and Landing WP but also other WP in the project. Task 2 represents

most of the work developed for this project. It is focused on the development of the landing sequence. In order to do this, several guidance algorithms will be considered in order to meet the requirements. The performance of these algorithms will have a huge impact in the general budgets of the mission, especially in the propellant mass budget and the  $\Delta V$  budget. In task 3 the hardware needed for the mission will be selected. When possible, Commercial off-the-shelf (COTS) components will be suggested in order to minimize low TRL related risks and minimize the overall cost of the mission.

### 1.3 Outline of the thesis organisation

In the second chapter of this report, the requirements of the mission will be presented and analysed. Some further analysis of the landing site will be carried out in this section. In chapter 3 an initial baseline for the descent will be updated and different landing strategies will be derived and analysed. From this analysis a descent mission scenario will be established. Chapter four will be focus on the GNC scheme and all the hardware needed for landing. A main propulsion system will be picked and some concrete sensors suitable for this mission will be suggested. Special attention will be put into the design of the mapping camera. In chapter 5, the development of a simulator for the whole descent will be described. With the results from that simulator, the performance of the chosen mission scenario will be assessed. Lastly, chapter 6 serves a conclusion of the whole project and future steps are suggested in case the project were to continue.

Besides the main body, 4 extra appendices are included. The first appendix is an executive summary of the work developed in this report. Then, a common appendix of the whole GDP project shows the relevant facts and figures for the whole mission, and not only relevant for descent and landing. A third appendix shows extra calculations to support the findings presented here. Finally, a compilation of the suggested sensors' datasheets is shown in appendix D.

# Chapter 2

## Requirements

### 2.1 Mission Statement

As part of a Group Design Project (GDP), the first task of the team was to analyse the information provided by Lunar Mission One in order to produce a mission statement and to derive the mission requirements. More information about this process can be found in [4]. The mission statement produced says:

*To design an spacecraft that is able to land and drill on the lunar surface before 2024, deposit a time capsule and perform in situ scientific experiment for the purpose of future scientific exploitation and human exploration within the budget of \$0.75 Bn*

From this mission statement we can derive the main top level requirements that will affect the Descent and Landing WP.

### 2.2 Descent and Landing Top-Level Requirements

As stated in [2], Lunar Mission One objective is to send a exploratory robotic mission to the south polar region of the Moon. This objective provide the Descent and Landing WP with its first requirement:

**R\_DL\_01** The spacecraft shall be able to land on the Lunar South Pole.

Once in the surface of the Moon, we want to perform in-situ science. When designing the landing sequence, we have to bear in mind that the spacecraft must be able to withstand the landing conditions. We also want to ensure that the spacecraft lands with the correct orientation (vertically) so all the instruments can operate correctly.

**R\_DL\_02** The spacecraft shall be able to withstand the landing conditions.

**R\_DL\_03** The spacecraft shall land vertically.

As this is an unmanned mission, direct control of the spacecraft during landing is not possible. The spacecraft must have built-in Hazard Detection and Avoidance (HDA) capabilities to achieve a safe landing on the Lunar South Pole.

**R\_DL\_04** The spacecraft shall be able to land autonomously.

With further analysis of the landing location and the mission, more requirements can be derived.

## 2.3 Landing Site Location

The reason behind choosing the Lunar South Pole as the landing area is due to its favourable illumination conditions with areas of almost continuous illumination and short periods of eclipse (50-70 hours) [5] and for its communication windows with the Earth, having a period of direct communication with Earth of 14 days followed by a non-communication window of 14 days [6]. In table 2.1, the top 5 potential landing sites from [6] are shown.

ID	Region Name	Longest Illumination Period [days]	Location (Lat/Lon [deg])
SR1	Shackleton Rim	274	(-89.7788, -153.4349)
SR2	Shackleton Rim	234	(-89.6871, -161.5651)
CR1	Connecting Ridge	316	(-89.4632, -137.4896)
MP1	Malapert Peak	196	(-85.9756, -2.1124)
MP2	Malapert Peak	203	(-86.0236, 2.6113)
LP1	Leibnitz beta Plateau	203	(-86.0236, 2.6133)

**Table 2.1:** Potential landing sites on the Lunar South Pole

Due to its proximity to the Shackleton Crater, one of the key targets for future scientific exploration [7], and its illumination conditions, the initial selected landing site is SR1 on the Shackleton Crater's Rim. The location of the landing site, with a latitude of -89.7788 degrees imposes a constraint in the Lunar Orbit inclination. To be able to orbit above that point, we must use a polar orbit ( $90^\circ$  of inclination) around the Moon.

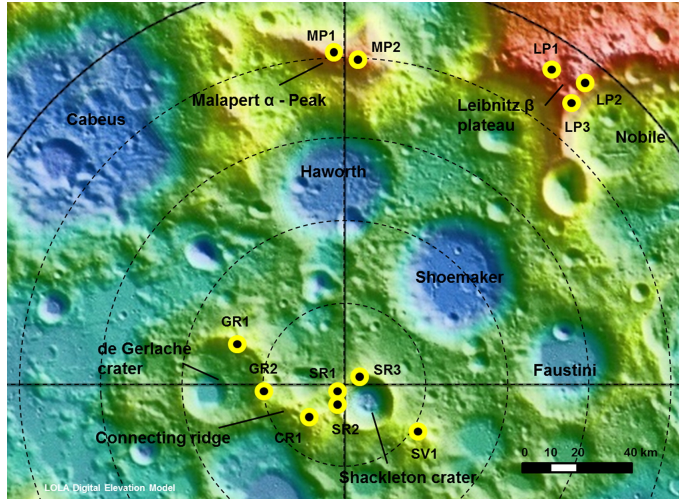


**Figure 2.1:** Location of potential landing sites in the Lunar South Pole [1]

From [6] we can also derive the needed accuracy to land in the desired landing location. To achieve the mentioned illumination conditions, we must be able to land inside a 200x200 m landing ellipse centred in the desired location. This requirement will be one of the main drivers in the design of the Descent Sequence.

**R\_DL\_05** The spacecraft shall be able to land inside a 200x200 m landing ellipse centred in the landing site.

As the information about the illumination conditions of the different landing locations come from simulations, we must be able to characterize these different areas previous to the landing to select the most suitable one. This will introduce new requirements. We must be able to perform an initial mapping of the Lunar South Pole and we must be able to change the landing site if desired. To minimize the risks of not being able to land due to an unexpected hazard, we want to be able to change the landing location not only prior to the beginning of the descent but also at any point during the landing sequence. The change of the landing site can be made automatically by the on-board computer based on information from the sensors, or manually from ground control.

**R\_DL\_06** The spacecraft shall be able to perform an initial mapping of the potential landing sites previous to landing.

**R\_DL\_07** The spacecraft shall be able to change the landing location at any point prior or during the landing sequence.

**R\_DL\_08** The spacecraft shall be able to communicate directly with Earth during the whole landing sequence.

# Chapter 3

## Descent Sequence

### 3.1 Introduction

In this chapter different concepts for the descent sequence will be proposed and studied in order to fulfil the requirements derived in chapter 2.

The first task to design the descent sequence is choosing between a soft landing powered by the engines or a hard landing, where the lander follows a trajectory that intersect with the Moon. Preliminary calculations for both scenarios can be found in appendices C.1.1 and C.1.2. As a first estimation, using a typical mission profile, to land a mass of 800 kg a soft landing would require a propellant mass of 717 kgs and a  $\Delta V$  of  $1929 \text{ m}\cdot\text{s}^{-1}$  while a hard landing would only require a  $\Delta V$  of  $23 \text{ m}\cdot\text{s}^{-1}$  and a propellant mass of 9.51 kg. However, the hard landing would need to dissipate 1159.8 MJ of energy at touchdown, while the energy to be dissipated in an ideal soft landing is theoretically 0.

	Soft Landing	Hard Landing
Propellant Mass [Kg]	717	9.51
$\Delta V [\text{m}\cdot\text{s}^{-1}]$	1929	23
Kinetic Energy [MJ]	0	1159.8

**Table 3.1:** Descent Preliminary Budgets

By looking at the propellant mass and  $\Delta V$  budgets shown in table 3.1, hard landing seems to be the desired option. However, the risks and constraints that an impact of such characteristics would introduce in the design of the mission make the hard landing a non-viable option. As past lander missions to the Moon such as the American Apollo program or the Russian Luna program, the option selected to land on the surface of the Moon is a soft landing.

By definition, a soft landing uses the propulsion system to achieve a zero velocity touchdown. As the spacecraft won't be designed to withstand impact velocities in

the order of the orbital speed, any substantial failure of the propulsion subsystem may result in a mission catastrophic failure. One of the main risks is known as “engine restart failure” [8], where the engine fails to reignite in the middle of the descent sequence, causing the lander to follow an uncontrolled trajectory that can potentially destroy the spacecraft on impact. To prevent this, we introduce a new requirement for the design of the landing sequence. This requirement will prevent the engines from turning off at any point of the descent sequence, meaning that no free fall trajectories are allowed in the descent sequence.

**R\_DL\_09** The engines of the spacecraft shall not be turned off at any point of the descent trajectory.

In the next sections the different landing strategies that can be used to fulfil all the requirements will be analysed in order to choose the best option or combination of them. To evaluate the performance of the different landing strategies we have to establish certain design drivers.

1. The landing strategy must fulfil all the mentioned requirements.
2. The landing strategy must minimize the total propellant mass.
3. The landing strategy must be able to be implemented in real time within the possibilities of existing technology.

The design driver number 3 is directly derived from the requirement of autonomous landing. All the control commands must be produced by the on-board computer which would have limited capabilities. To ensure a successful landing, the commands must be produced quickly. For this reason, analytical algorithms are preferred over long iterative algorithms with slow convergence rates.

In conclusion, the design of the descent sequence is an optimization problem where we want to minimize the propellant mass while achieving all the mentioned requirements and ensuring real time implementation.

## 3.2 Descent Baseline

In this section we will establish a first baseline for the design of the descent sequence. This baseline will constraint the design space for the optimization problem.

From the operations work package [9] the requirement of landing at the beginning of the Lunar Summer cycle is imposed. To be more precise, the landing date selected is the 28th of September of 2024. It has been already stated that, prior to the landing, we need to map potential landing sites of Lunar South Pole. That mapping would help not only to asses the feasibility of the landing site but it will also serve as a training for our navigation sensors <sup>1</sup>.

---

<sup>1</sup>The sensors will be discussed in chapter 4

To minimize propellant consumption, the lunar orbit shall pass directly above the landing site. After the mapping, the information obtained will be analysed. The period of time needed for the analysis of this information will cause the landing site to move away from the orbit track due to the Moon rotation. To achieve again the same geometric conditions between the spacecraft velocity direction and relative position respect to the landing site, the spacecraft shall wait in a Lunar Parking Orbit during a full rotation of the Moon (27.32 days).

The next step in the design process is picking the altitude above the lunar surface to begin the descent sequence. To save propellant, we want to choose the minimum safe altitude. Taking into account the highest peak over the lunar surface [10], we peak an altitude of 15 km. In order to have more flexibility respect to the landing site, a circular orbit around the Moon is ideal (taking advantage of the Moon rotation, we could theoretically land in any part of the Moon with a similar propellant consumption from a circular orbit).

From this analysis, the ideal situation would be to have a circular orbit of 15 km around the Moon. That low orbit would allow us to have a precision mapping of the lunar South Pole and any other interesting areas and minimize the propellant mass needed from landing. However, an orbit with that altitude is unstable and the perturbations would make the altitude quickly decay during the parking orbit, resulting in a collision risk for the lander.

Working in close collaboration with the Orbits Work Package [11] and after several iterations, the following scenario has been picked.

1. Initial elliptical lunar mapping orbit with 100 km apoapsis altitude and 15 km periapsis altitude.
2. Transfer into a circular parking orbit with an altitude of 100 km. Wait in the parking orbit until the same geometric conditions as the mapping orbit have been achieved (1 full rotation of the Moon).
3. Transfer into an elliptical descent orbit with 100 km apoapsis altitude and 15 km periapsis altitude.
4. Beginning of the descent sequence at the periapsis of the descent orbit (15 km of altitude).

### 3.3 Modelling of the dynamics of the lander

Prior to any optimization, it is needed to model the dynamics of the spacecraft.

As a first approximation, we can uncouple the attitude control, that will be studied by the AOCS Work Package [12] from the translational problem.

The equations of motion of the spacecraft will be derived using a Moon Centered Inertial frame of reference. The kinematic and dynamic equations are derived as follows [13] using the spherical coordinate system of figure 3.1.

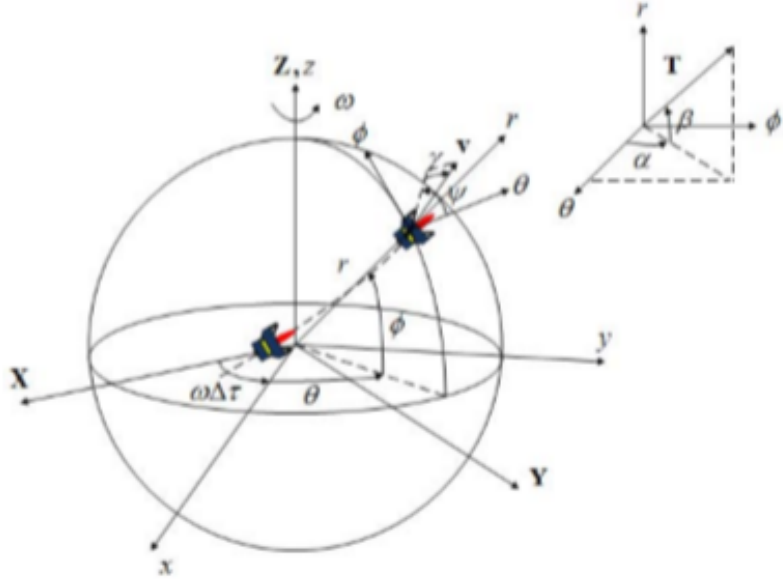


**Figure 3.1:** Spherical coordinate system used in the equations of motion

$$\dot{r} = v_r \quad (3.1)$$

$$\dot{\theta} = \frac{v_\theta}{r \cos \phi} \quad (3.2)$$

$$\dot{\phi} = \frac{v_\phi}{r} \quad (3.3)$$

$$\dot{v}_r = \frac{-T_{max}k}{m} \sin \beta - \frac{\mu_M}{r^2} + \frac{v_\phi^2}{r} + \frac{v_\theta^2}{r} + r\omega_M^2 \cos \phi \quad (3.4)$$

$$\dot{v}_\theta = \frac{T_{max}k}{m} \cos \beta \cos \alpha - \frac{v_r v_\theta}{r} + \frac{v_\theta v_\phi \sin \phi}{r \cos \phi} + 2\omega_M v_\phi \sin \phi - 2\omega_M v_r \cos \phi \quad (3.5)$$

$$\dot{v}_\phi = \frac{T_{max}k}{m} \cos \beta \sin \alpha - \frac{v_r v_\phi}{r} - \frac{v_\theta^2 \sin \phi}{r \cos \phi} - r\omega_M^2 \sin \phi \cos \phi - 2\omega_M v_\theta \sin \phi \quad (3.6)$$

where  $\omega_M$  is the mean angular velocity of the Moon ( $2.662 \text{ rad}\cdot\text{s}^{-1}$ ) and  $T_{max}$  the maximum thrust of the engine. The control parameters of the spacecraft are the throttle command  $k$  and the attitude of the spacecraft, represented by the control angles  $\alpha$  and  $\beta$ . In the poles, and due to the low value of  $\omega_M$ , the velocity induced by the rotation of the Moon is negligible. Equations 3.4, 3.5 and 3.6 can be simplified as:

$$\dot{v}_r = \frac{-T_{max}k}{m} \sin \beta - \frac{\mu_M}{r^2} + \frac{v_\phi^2}{r} + \frac{v_\theta^2}{r} \quad (3.7)$$

$$\dot{v}_\theta = \frac{T_{max}k}{m} \cos \beta \cos \alpha - \frac{v_r v_\theta}{r} + \frac{v_\theta v_\phi \sin \phi}{r \cos \phi} \quad (3.8)$$

$$\dot{v}_\phi = \frac{T_{max}k}{m} \cos \beta \sin \alpha - \frac{v_r v_\phi}{r} - \frac{v_\theta^2 \sin \phi}{r \cos \phi} \quad (3.9)$$

Lastly, we need to model propellant mass flow through the engine.

$$\dot{m} = -\frac{k T_{max}}{I_{sp}} \quad (3.10)$$

Here it is shown that the motion of the spacecraft during the descent is governed by a set of non-linear differential equations. In general, no analytical solution can be obtained for the integration of these equations except in the most trivial cases. These equations have to be integrated using numerical methods. In general, a Runge-Kutta scheme of 4th order has been used.

### 3.4 Descent Strategies

With the base of equations 3.1 to 3.3 and 3.7 to 3.10, different landing guidance laws have been implemented and tested.

For the study of the landing strategies, the following considerations have been taking into account:

1. The descent sequence begins at 15 km above the Moon surface with the spacecraft travelling at orbital speed. The downrange to the landing site is one of the design parameters.
2. To prevent the engine restart failure, the engine throttle minimum position is limited at 0.2. Also, to have manoeuvrability margin against unexpected events the throttle maximum position is limited at 0.9. To sum up  $k$  varies between [0.2, 0.9].
3. Hazard avoidance and detection is one of the keys to a successful landing. For this reason, the descent sequence will finish with the lander hoovering vertically over the landing site at 100 m and descending at a constant vertical velocity of  $-5 \text{ m}\cdot\text{s}^{-1}$ . In this phase, horizontal displacement for hazard avoidance or final precision landing can be achieved using the reaction control thrusters of the attitude control subsystem.

The studied guidances laws are:

1. Direct Collocation Methods.
2. Gravity Turn.
3. Zero-Effort-Miss/Zero-Velocity Miss (ZEM/ZEV) improved using Model Predictive Static Programming (MPSP).
4. Optimal Control Theory and the Pontryagin's Maximum Principle.

### 3.4.1 Direct Collocation Methods

In [13] and [8] direct optimization using collocation methods are proposed for the descent trajectory design. The approach of the direct collocation methods is to discretize the continuous optimal control problem into a series of  $N$  points or Nodes along the descent trajectory. At each of those nodes  $i = 1, 2, \dots, N$ , we want to find the attitude ( $\alpha_i$  and  $\beta_i$ ) and the throttle command ( $k_i$ ) that maximizes the landed mass. Besides finding the control parameters along the trajectory, the solution algorithm also has to find the other design parameters such as initial range to the landing site, the total descent time and the engine maximum thrust. The total number of design parameters is:

$$\text{Design Parameters} = 3N + 3 \quad (3.11)$$

The equations of motions are integrated numerically and the control parameters are propagated between the nodes using piecewise-continuous functions such as Lagrange polynomials [14].

The strength of this method is that, if successfully implemented, it allows to compute the global optimal solution of the problem. The main drawback is that the optimization solution techniques such as conjugated gradient usually require a lot of iterations and computational effort. To solve this problem, software packages specialized in non-linear optimal control such as DIDO is used.

A first attempt using a similar approach with MATLAB's function *fmincon* was made. To achieve an accurate representation of the optimal solution it is needed to use a substantial number of nodes (the optimal solution can only be achieved with  $N = \infty$ ). With a representation of the trajectory with only 20 nodes (taking as a reference the 500 s that lasted the Apollo descent [15] that would mean one control node each 25 s) we have an optimization problem of dimension 63. The computational effort needed to solve the non-lineal optimization problem without any further simplifications soon become unbearable without the assistance of more specialized software.

### 3.4.2 Gravity turn

The gravity turn is one the most simple optimal control strategies that can be used for descent and landing. This fuel efficient guidance law points the thrusts against the instantaneous velocity at every point of the trajectory. Due to the effect of the gravity (acting in a radial direction from the centre of the Moon), it assures that the spacecraft will land vertically on the Moon.

The main drawback of this strategy is that it does not fully fulfil the requirements, as it has no retargeting capabilities. It cannot also achieve the desired accuracy required for the landing.

Besides this drawbacks, is an interesting strategy that efficiently removes the orbital velocity while minimizing the propellant mass. It is also very easy to implement, as the spacecraft attitude control only has to align the thrust vector with the velocity measured by sensors such as Inertial Measurement units. It can be used in a initial braking phase of the descent trajectory.

### 3.4.3 Zero-Effort-Miss/Zero-Velocity-Miss algorithm improved using Model Predictive Static Programming

The Zero-Effort-Miss/Zero-Velocity-Miss (ZEM/ZEV) algorithm is a guidance law derived from the proportional navigation law used in missile guidance [16]. It has been widely considered as a guidance law for the precision terminal landing phase of space missions to the Moon, Mars, asteroids or other celestial bodies [17–19].

The ZEM/ZEV algorithm is a near-optimal feedback guidance law. Under certain assumptions of the gravity force field the control commands produced by this algorithm can be derived analytically with the use of simple expressions, making it desirable to save computational effort in autonomous landings.

The complete derivation of the algorithm can be found in [20]. A brief explanation of how it works will be given here. The target of this guidance algorithm is to place the spacecraft at certain final position  $\mathbf{r}_f$  with certain final velocity  $\mathbf{v}_f$  in a given time  $t_f$ . The total duration  $t_f$  is usually the design parameter of the algorithm. In order to do so at each time  $t$ , and with the information of its current position  $\mathbf{r}(t)$  and  $\mathbf{v}(t)$  it computes the projected final position and velocity if no controls (no thrust in this case) were applied  $\mathbf{r}_{nc}$ ,  $\mathbf{v}_{nc}$ . If we consider gravity as the dominant force and neglect other perturbations:

$$\mathbf{r}_{nc} = \mathbf{r}(t) + (t_f - t)\mathbf{v}(t) + \int_t^{t_f} \int_t^{t_f} \mathbf{g}(\tau) d\tau d\sigma \quad (3.12)$$

$$\mathbf{v}_{nc} = \mathbf{v}(t) + \int_t^{t_f} \mathbf{g}(\tau) d\tau \quad (3.13)$$

The **ZEM** is for how far will the spacecraft miss the desired position and the **ZEV** vector is how big will the velocity error be if no command is applied after the present time. If we assume a constant gravity (reasonable when we are in the vicinity of the landing site) that does not depend on the position or time, the expressions for **ZEM** and **ZEV** can be easily obtained.

$$\mathbf{ZEM} = \mathbf{r}_f - \mathbf{r}_{nc} = \mathbf{r}_f - \left( \mathbf{r}(t) + t_{go}\mathbf{v}(t) + \frac{1}{2}t_{go}^2\mathbf{g} \right) \quad (3.14)$$

$$\mathbf{ZEV} = \mathbf{v}_f - \mathbf{v}_{nc} = \mathbf{v}_f - (\mathbf{v}(t) + t_{go}\mathbf{g}) \quad (3.15)$$

Where  $t_{go}$  is simply remaining time of the trajectory

$$t_{go} = t_f - t \quad (3.16)$$

We feedback this quantities to the algorithm to compute the needed commands to make them 0. The commands are computed using optimal control theory. If the gravity is a explicit function of time only (or constant), the optimal control problem using has an analytical solution [18] for the commanded acceleration (an attitude, as it is the acceleration in the three reference axis).

$$\mathbf{a}(t) = \frac{\mathbf{T}(t)}{m(t)} = \frac{6}{t_{go}^2} \mathbf{ZEM} - \frac{2}{t_{go}} \mathbf{ZEV} \quad (3.17)$$

Equation 3.17 shows how the control commands can be easily computed analytically. They depend only of the  $t_{go}$ , the actual state vector and the desired position. Besides saving computational effort, it also has re-targeting capabilities, as we can change the desired final position and/or velocity at any point.

The generalized ZEM/ZEV algorithm does not take into account any thrust level constraints. Besides that, optimal trajectories usually have a part of subsurface flight. That would cause our lander to crash with the Moon. To avoid that [21] proposes a improved version of the ZEM/ZEV algorithm using Model Predictive Static Programming. It first generates a ZEM/ZEV trajectory with the thrust level constraint. Then if, because of the constraint, the final position or velocity are not met or if there are any subsurface flight paths, it iteratively uses static programming optimization theory to met all the constraints. The Model Static Predictive Programming has high computational efficiency as part of the solutions have a closed analytical form and the matrix needed for the iterations can be computed recursively.

This algorithm has been coded and tested for our particular problem. In figure 3.2 a descent trajectory generated using the improved ZEM/ZEV algorithm with MPSP is shown.

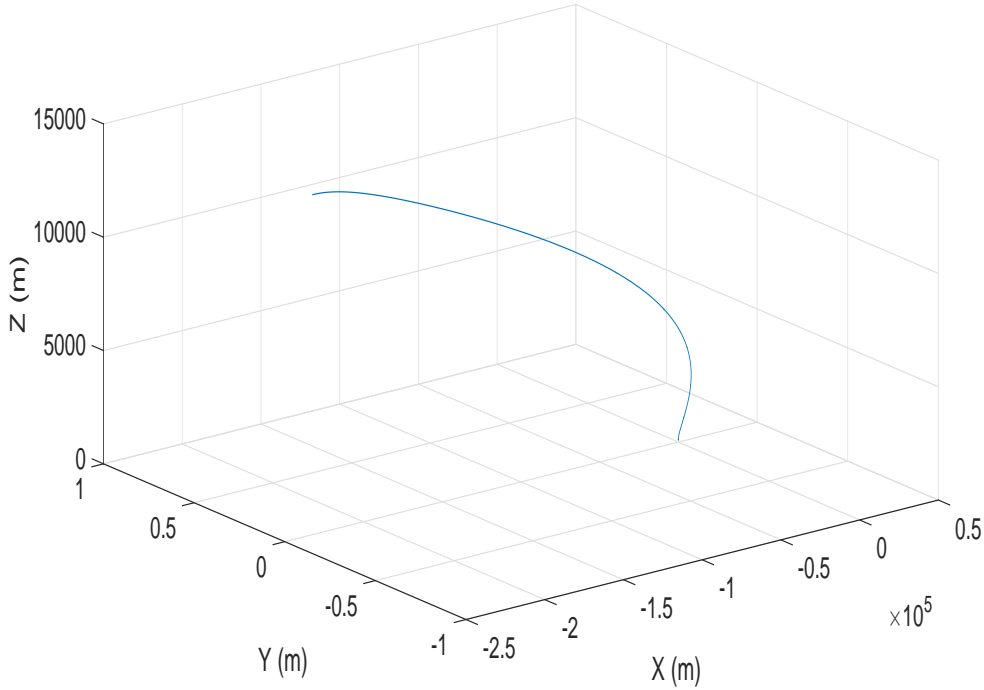


**Figure 3.2:** 3D representation of the descent trajectory generated using the Improved ZEM/ZEV with MPSP

Some of the relevant parameters for this trajectory are shown in table 3.2.

Total time [s]	Maximum Thrust [N]	Propellant Mass [Kg]	$\Delta V$ [m·s <sup>-1</sup> ]	Iterations to converge [-]
400	15000	700	2128	3

**Table 3.2:** Parameters of the trajectory using the improved ZEM/ZEV algorithm with MPSP

The algorithm converges quickly towards the solution, needing only three iterations, so real time implementation can be achieved. As it is a feedback algorithm, high precision can be achieved. The maximum thrust level allowed here was 15000 N. Revising existing and past engine technologies with throttling capabilities [22], this value is too high for this particular problem. The main drawback of this improved ZEM/ZEV algorithm is the high thrust requirements that it imposed. When used with more realistic values of thrust level (from 1 to 5 kN) the convergence time rapidly increases (from 2 or 3 iterations to hundreds or thousands of them) and the process can even diverge, making it unfeasible for real time implementation. This behaviour is due to the high initial velocity compared to the final velocity and the high mass in this particular case. When applied to lower masses and velocities, the high thrust requirements disappear.

The re-targeting capabilities and the high accuracy of this feedback algorithm make it appropriate to achieve a high precision soft landing as the one required here. However, the thrust level required make it inapplicable for a real time implementation as the only guidance law. This algorithm is more suitable for the final precision landing phase rather than for the whole descent phase.

### 3.4.4 Optimal Control Theory

Finally, it has been taken into consideration the possibility of applying the techniques of optimal control theory and variational calculus to develop other control laws. Specifically, we have applied the *Pontryagin's Maximum Principle* to develop a control law for the initial phase of the descent. This principle says that, in order to maximize a certain function (the landed mass in this case) dependant of the trajectory followed by a dynamical system, the controls applied must maximize the Hamiltonian at each point of the trajectory. A formal definition of the *Pontryagin's Maximum Principle* can be found in [23].

A brief description of the derivation of the control law is given here. The following assumptions for the model are made:

1. The descent elliptical orbit passes directly above the chosen landing site.
2. From 1, and knowing that the orbital velocity is contained in the trajectory plane [24], we can restrict the motion to the orbital plane having a 2D problem instead a 3D.
3. The state of the system is described by two positions measures  $r$  and  $\phi$ , two velocities  $v_r$  and  $v_\phi$  and the mass  $m$ .

$$\mathbf{x} = \begin{Bmatrix} r \\ \phi \\ v_r \\ v_\phi \\ m \end{Bmatrix} \quad (3.18)$$

4. The thrust vector is always contained in the motion plane.
5. The state is now controlled by the throttle magnitude  $k$  and only one attitude angle  $\beta$ .

$$\mathbf{u} = \begin{Bmatrix} k \\ \beta \end{Bmatrix} \quad (3.19)$$

6. The polar coordinate system and the angles definition can be seen in figure 3.3.
7. We want to maximize a certain functional  $\Upsilon$ , which consist in the landed mass

$$\Upsilon = m \quad (3.20)$$

The differential equations of the problem are:

$$\dot{r} = v_r \quad (3.21)$$

$$\dot{\phi} = \frac{v_\phi}{r} \quad (3.22)$$

$$\dot{v}_r = \frac{v_\phi^2}{r} - \frac{\mu_M}{r^2} + \frac{kT_{max}}{m} \sin \beta \quad (3.23)$$

$$\dot{v}_\phi = -\frac{v_r v_\phi}{r} + \frac{kT_{max}}{m} \cos \beta \quad (3.24)$$

$$\dot{m} = -\frac{kT_{max}}{I_{sp}} \quad (3.25)$$

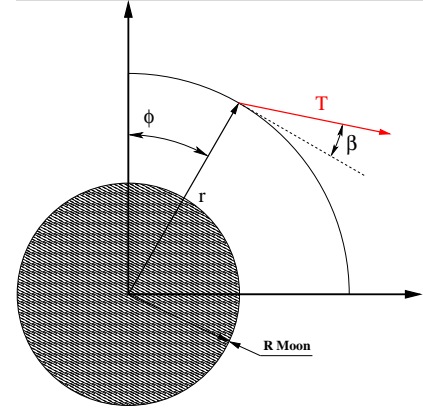


**Figure 3.3:** Coordinate system and angles definition

The following boundary conditions are applied

Initial conditions:

Terminal conditions <sup>2</sup>:

$$r(t_0) = r_0 \quad (3.26) \quad \psi_r = r(t_f) - r_f = 0 \quad (3.31)$$

$$\phi(t_0) = \phi_0 \quad (3.27) \quad \psi_\phi = 0 \quad (\text{Free}) \quad (3.32)$$

$$v_r(t_0) = v_{r0} \quad (3.28) \quad \psi_{v_r} = v_r(t_f) - v_{r_f} = 0 \quad (3.33)$$

$$v_\phi(t_0) = v_{\phi0} \quad (3.29) \quad \psi_{v_\phi} = v_r(t_f) - v_{\phi_d} = 0 \quad (3.34)$$

$$m(t_0) = m_0 \quad (3.30) \quad \psi_m = 0 \quad (\text{Free}) \quad (3.35)$$

We can compute the Hamiltonian  $H$  by defining the costate vector  $\mathbf{p}$

$$\mathbf{p} = \begin{Bmatrix} p_r \\ p_\phi \\ p_{v_r} \\ p_{v_\phi} \\ m \end{Bmatrix} \quad (3.36)$$

$$\begin{aligned} H(p, x, u, t) = \mathbf{p}^T \dot{\mathbf{X}} &= p_r v_r + p_\phi \frac{v_\phi}{r} + p_{v_r} \left( \frac{v_\phi^2}{r} - \frac{\mu_M}{r^2} + \frac{kT_{max}}{m} \sin \beta \right) \\ &\quad + p_{v_\phi} \left( -\frac{v_r v_\phi}{r} + \frac{kT_{max}}{m} \cos \beta \right) + p_m \left( -\frac{kT_{max}}{I_{sp}} \right) \end{aligned} \quad (3.37)$$

The costate equations can be derived obtained from [23]

$$\dot{p}_i = -\frac{\partial H}{\partial x_i} \quad (3.38)$$

<sup>2</sup>The Pontryagin's maximum principle need to set zero terminal conditions affecting at each state variable to compute the costates. The final state of a variable can be free, in which case the terminal condition will be directly zero [23]

In our problem, this lead to:

$$\dot{p}_r = p_\phi \frac{v_\phi}{r^2} - p_{v_r} \left( -\frac{v_\phi^2}{r^2} + \frac{2\mu_M}{r^3} \right) - p_{v_\phi} \frac{v_r v_\phi}{r^2} \quad (3.39)$$

$$\dot{p}_\phi = 0 \quad (3.40)$$

$$\dot{p}_{v_r} = -p_r + p_{v_\phi} \frac{v_\phi}{r} \quad (3.41)$$

$$\dot{p}_{v_\phi} = -\frac{p_\phi}{r} - 2p_{v_r} \frac{v_\phi}{r} + p_{v_\phi} \frac{v_r}{r} \quad (3.42)$$

$$\dot{p}_m = p_{v_r} \frac{kT_{max}}{m^2} \sin \beta + p_{v_\phi} \frac{T}{m^2} \cos \beta \quad (3.43)$$

As stated in the Pontryagin's maximum principle the optimal control  $\mathbf{u}^*$  belonging to the subspace of admissible controls  $\mathcal{U}$  maximizes the Hamiltonian at each time of the trajectory

$$\mathbf{u}^* = \max_{u \in \mathcal{U}} H(p, x, u, t) \quad (3.44)$$

In [25] is proved that only bang-bang profiles are optimal (the throttle either is maximum or minimum) with different combinations of one arc (max or min), double-arc (max-min or max-min) etc. For our application a single arc is chosen. The engines will be at full thrust for the whole manoeuvre.

$$k = k_{max} \quad (3.45)$$

The only remaining parameter of the control is the optimal attitude angle  $\beta^*$ . This angle must maximize the Hamiltonian

$$\frac{\partial H}{\partial \beta} = 0 \quad (3.46)$$

$$p_{v_r} \frac{kT_{max}}{m} \cos \beta - p_{v_\phi} \frac{T}{m} \sin \beta = 0 \quad (3.47)$$

The optimal attitude angle  $\beta^*$  is

$$\beta^* = \tan^{-1} \frac{p_{v_r}}{p_{v_\phi}} \quad (3.48)$$

From [23] we know that the final values of the costates must fulfil certain transversality conditions, where  $\nu_i$  are unknown parameters.

$$p_i + \nu_i \frac{\partial \psi}{\partial x_i} + \frac{\partial \Upsilon}{\partial x_i} \quad t = t_f$$

Applied to  $p_\phi$  and as the final value of  $\phi$  is a free parameter ( $\psi_\phi = 0$  and the functional  $\Upsilon$  does not depends explicitly of  $\phi$ ) we found that

$$p_\phi(t = t_f) = 0 \quad (3.49)$$

From 3.40 and 3.49 it is trivial to derive that:

$$p_\phi = 0 \quad \forall t \quad (3.50)$$

The  $p_m$  equation is uncoupled with the rest of the equations and it does not appear in the optimal control. It is not necessary to solve it. This is because under the conditions of 3.45, the maximum landed mass is equivalent to a minimum time problem. The minimum propellant consumption for the landing is minimized by minimizing the total manoeuvre time.

The optimal control problem is now reduced to solve the following differential equations:

$$\dot{p}_r = p_\phi \frac{v_\phi}{r^2} - p_{v_r} \left( -\frac{v_\phi^2}{r^2} + \frac{2\mu_M}{r^3} \right) - p_{v_\phi} \frac{v_r v_\phi}{r^2} \quad (3.51)$$

$$\dot{p}_{v_r} = -p_r + p_{v_\phi} \frac{v_\phi}{r} \quad (3.52)$$

$$\dot{p}_{v_\phi} = -2p_{v_r} \frac{v_\phi}{r} + p_{v_\phi} \frac{v_r}{r} \quad (3.53)$$

$$(3.54)$$

and knowing that

$$\beta^* = \tan^{-1} \frac{p_{v_r}}{p_{v_\phi}} \quad (3.55)$$

$$k = k_{max} \quad (3.56)$$

The only unknown from this set of differential equations seem to be the three initial values of the costates. However, due to the linearity of the Hamiltonian 3.37 with respect to the costate, we can fix one of the costate's initial value and the other two will simply be rescaled. For this guidance law, only two unknowns remains, the initial value of two costates. These have to be chosen in order to achieve the desired final values for position and velocity.

An optimal descent control law has been derived in this section. In this strategy, the engines are fired at full thrust for the whole manoeuvre and a set of three coupled non-linear differential equations must be integrated at each step to compute the attitude control command. The integration of equations 3.51-3.53 have no analytical solution and need to know the state of the spacecraft (position, velocity and mass) at each instant of time. This information has to be provided by sensors. The integration of these equations can be easily done numerically using, for example, a Runge-Kutta integration scheme. As it uses the engines at full thrust, this strategy is suitable to efficiently remove most of the orbital velocity while saving propellant mass in an initial braking phase, but not for the final precision landing phase.

### 3.5 Mission scenario for the descent

In section 3.4 different landing strategies have been analysed in terms of its suitability for our particular problem. The direct collocation method can potentially achieve the global optimal solution. However, it requires a lot of computational effort and specialized software to be developed. The gravity turn is a simple manoeuvre that can be used for a soft landing. However, it does not fulfil the requirements for Lunar Mission One. The ZEM/ZEV algorithm is suitable for use as the final control law, to achieve a high precision landing on the Moon, but it cannot be realistically used at the beginning of the descent due to the high orbital velocity. Finally, we have applied optimal control theory to derive a control law that is suitable to be used in an initial braking phase of the descent sequence.

The final chosen descent scenario is split in three different parts. In each part a different control law is used with a specific design driver behind. The mission scenario has been summarized in table 3.3.

Phase	Name	Control Law	Design Driver
1	Braking Phase	Optimal Control	Kill orbital velocity Reduce Propellant Consumption
2	Approach Phase	ZEM/ZEV Algorithm	High Accuracy Re-targetting Capabilities
3	Vertical Descent	Constant Velocity Descent	Hazard Detection and Avoidance

**Table 3.3:** Descent Mission Scenario

More specific details about the final descent sequence are discussed in 5

# Chapter 4

## Hardware for descent and landing

### 4.1 Introduction

In this section, all the hardware requirements of the mission for the descent and landing will be picked. The hardware needed for landing can be divided into three main parts:

1. Propulsion system. In particular the main engine system. The reaction control thruster for three axis attitude control will be picked by the AOCS WP [12].
2. Mapping hardware. A sensor for the initial mapping of potential landing sites is needed.
3. The GNC hardware. A GNC scheme for the descent is proposed and the needed sensors are recommended.

As LMO is a crowdfunded mission with limited resources, when possible, the design of new sensors has been avoided and COTS components with proven space heritage have been picked to reduce low TLR risks and keep the development costs as low as possible. Only a full preliminary design had to be done for the mapping camera, as no complete information of cameras with similar requirements could be found.

## 4.2 Main Engine Selection

An initial sizing of the minimum thrust needed for the descent can be made by calculating the thrust needed to counteract the weight of the lander in the final vertical descent. The gravity on the lunar surface is  $g_M = 1.62 \text{ m}\cdot\text{s}^{-2}$ . The dry mass of the lander is estimated in 800 kg. The minimum thrust required for the mission is:

$$T_{min} = mg_M = 1296 \text{ [N]} \quad (4.1)$$

The value of 4.1 is the absolute minimum to achieve a soft landing. From previous calculations, it has been already estimated that the propellant mass required for landing is of the same order as the total dry mass. In 3.4.4 we have stated that the minimum propellant mass is achieved with a minimum time manoeuvre. As the initial velocity is already fixed by the orbits selected, the time can only be reduced by incrementing the thrust. The main engine will serve as one of the controls for the landing, adjusting its thrust level in the approach phase. For this reason we need a throttatable engine.

To sum up, for the main engine a compact system with high thrust, high performance in terms of low propellant consumption (high  $I_{sp}$ ) and throttability capabilities is needed. All this reasons led us to pick a liquid bi-propellant system as the main propulsion system [26]. An iterative process using the descent algorithms explained in 3 to choose an optimal configuration. The final configuration uses 4 Aerojet R-42DM with a nominal thrust of 890 N. More information can be found in appendix D.1. The main characteristics of the engine are summarized here [27].

Nominal Thrust [N]	890
$I_{sp}$ [s]	327
Thrust range [N]	356 - 1334
Propellant	Hydrazine/NTO(Mon-3)
Oxidizer/Fuel ratio	0.8-1.2

**Table 4.1:** Characteristics of the Aerojet R-42DM



**Figure 4.1:** Aerojet R-42DM

## 4.3 Mapping camera

As stated before, previous to the landing an initial mapping of different potential landing sites will be carried out. In order to do so, in the mission baseline a mapping orbit has been included. This mapping orbit will have similar parameters as the final descent elliptical orbit with an altitude of periapsis of 15 km and an altitude of the apoapsis of 100 km. Besides mapping potential landing sites to asses its characteristics, this mapping orbit will also serve as a training sequence for the rest of the navigation sensors, so it is important that when the actual landing begins, the geometrical and illumination conditions are as similar as possible to reduce errors. To achieve this, a full rotation of the Moon is needed between the mapping and the descent orbits.

With the mapping, we want to asses the feasibility of the landing sites in terms of possible hazards (big slopes, craters, rocks etc) and illumination conditions. For this reason, we need high spatial resolution (at least of the same order of the lander footprint) and the use of an optical imager.

The requirements of the imager are:

1. High spatial resolution
2. Wide field of view
3. High accuracy
4. Minimum mass and power consumption

The parameters of the camera has been estimated following the observation payload design process of [28]. All the relevant parameters of the design can be found in appendix C.2. The operating wavelength of the imager has been set in the middle of the visible spectrum ( 540 nm) with a spectral bandwidth that covers all the visible spectrum. As a detector, a CCD array with 4096x4096 pixels of  $5.5 \mu\text{m}$  yields a FOV of 38.95 deg. This allow us to achieve a spatial resolution at nadir of 2.5 m over a swath width of 10018 m. The lander footprint is estimated to be around 4 m, so this spatial resolution is enough for an initial detection of potential landing sites. For more precise selection of the final landing site, the hazard and detection algorithms and also direct manual control can select the precise landing location in the final stages of the descent sequence. In this stages, the lander will be hoovering above the landing site with an altitude of 100 m enabling to acquire higher resolutions images to avoid small rocks and undetected slopes.

Parameter	Value	Units
Operating Wavelength	540	nm
Bandwidth	400	nm
CCD array size	4096x4096	pixels
Detector size	5.5	$\mu m$
FOV	38.96	deg
Spatial Resolution	2.5	m
Swath Width	10018	m

**Table 4.2:** Characteristics of the mapping imager

To achieve this performance, a lens with a focal length of 331 mm is needed. The diffraction limited aperture for an imager with this characteristics is 2.71 mm. An aperture of 3.68 mm has been selected, yielding an F# of 9, enough for this application.

Parameter	Value	Units
Focal length	331	mm
Aperture	3.68	mm
F#	9	

**Table 4.3:** Sensor Optics

The next step is to evaluate the pointing accuracy and stability requirements needed to obtain high quality images. This requirements will have to be met by the Attitude Control subsystem. Taking into account an altitude of 15 km and a spatial resolution of 2.5 m, having a 0.5% accuracy on ground for a 10 km swath width means that the mapped area can be either 50 m either size of the swath width:

$$\tan(\theta + \delta\theta) - \tan(\theta) = \tan \frac{5124}{15000} - \tan \frac{5098}{15000} \quad (4.2)$$

$$\delta\theta \approx 0.1 \text{ deg} \quad (4.3)$$

For an initial mapping of potential landing sites, a pointing accuracy of 0.1 deg is needed.

### 4.3.1 Mapping Camera Sizing

The characteristics of the designed camera are similar to the Osiris Camera of the Rosetta Mission [29] and the camera on board the Chinese mission to the Moon Chang'e 2 [30] that are able to acquire images with similar spatial resolutions. Unfortunately, no complete data about mass, dimensions and power are available. To

estimate those parameters, we will scale down from existing instruments as suggested in section 17.2.6 of [28].

The instrument that will serve as a reference is the Mars Descent Imager Camera MARDI [31], whose characteristics are presented in table 4.4

Aperture Diameter [mm]	Mass [kg]	Power [W]	Dimensions [mm]
2.6	0.405	10	90x63x86

**Table 4.4:** Budget of MARDI camera

The ratio between aperture diameters ( $D$ ) for both instruments is

$$R = \frac{D_{\text{design}}}{D_{\text{MARDI}}} = 0.637 \quad (4.4)$$

Using this ratio and following [28], the instrument main parameters are:

Mass [kg]	Power [W]	Dimensions [mm]
1.15	28.4	127x89.2x122

**Table 4.5:** Budget of the mapping camera

## 4.4 Guidance Navigation and Control Scheme

The Guidance, Navigation and Control scheme is partially based in the developments by the ESA's Lidar-based Autonomous Planetary landing System (LAPS) [32] and Nasa's Autonomous Landing and Hazard Avoidance Technology (ALHAT) [33]. Both of this projects are developing the technology for future planetary landing mission. This technology is based in the use of Lidar sensors, instead of radar, in combination with new Hazard Detection and Avoidance Algorithms.

Due to the limitation in time and resources of the project, the study of the Hazard Avoidance and Detection Algorithms and its performance is out of the scope of this project. However, a simple layout of the GNC scheme is proposed for this mission. The GNC scheme proposed is composed of

- Inertial Measurement Units (IMU).
- Optical cameras.
- Lidar Cameras.

- Lidar Velocimeter and Altimeter.

For the whole descent, inertial navigation will be used. The position, velocity and attitude of the lander will be known from the measures coming from the gyros and accelerometers of the IMUs. However, a high resolution model of the gravity field in the Moon is need to avoid errors in the state estimation. To avoid these errors and the unavoidable noise of any real sensor, this measures will be processed using Kalman filtering techniques and updated with external measures coming from other sensors such as Lidar and optical cameras and velocimeters. A diagram of the proposed configuration is shown in figure 4.2.

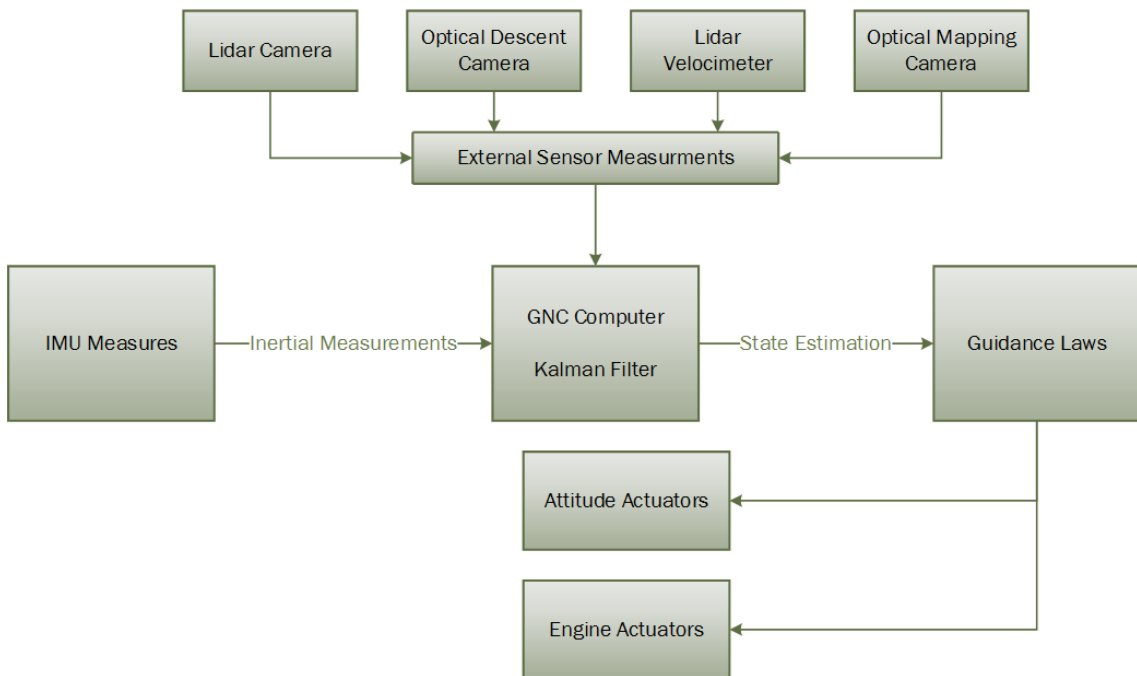


**Figure 4.2:** Proposed GNC scheme for the descent

Three IMU's will be used for the inertial navigation. Two of the IMU's will be redundant, and a logic of three will be used in case there is any mismatch between estimations. To avoid all three IMU's having the same failure modes, one of the IMU's will come from a different manufacturer. Both models of IMU's have proven space heritage in lander mission, as they have been used in the Mars Science Laboratory (Curiosity).

The mapping camera can be used in the initial stage to perform optical terrain relative navigation. The images taken in the initial mapping serve as a training sequence for navigation in the descent. This camera will be mounted on the side of the lander facing down to nadir in the initial descent. More information on the location of this and other sensors can be found from the configuration work package [34].

One flash Lidar camera will perform Terrain Relative Navigation, Hazard Detection and Avoidance and, as secondary function, Altimetry measurements. The flash

Lidar camera selected is the DragonEye manufactured by Advanced Scientific Concepts. This model is involved in the ALHAT project and has been successfully tested in docking operations in the ISS. The operational range of this camera is up to 4 km, so it will be used in the approach phase of the descent. This camera will be mounted on a gimbal platform on the side of the lander that allow it to point both vertical downwards and to the side of the lander.

One optical descent camera. This camera will be mounted in the bottom of the spacecraft facing down. It will be used for optical terrain relative navigation in the final part of the descent. The camera selected is the Mars Descent Imager, used in missions such as Mars Science Laboratory or Mardi. Minimum modifications will have to be made to adapt it for Moon use. The capability of recording high resolution color video of the final descent not only has high engineering value but also is an added feature for public engagement of the mission.

Finally, a doppler Lidar Velocimeter will perform Velocimetry and Altimetry functions. The Lidar based sensor is manufactured by efacec.

For our lander, the main hazards are the slopes, rocks and shadows, as landing in a non-illuminated area would mean a catastrophic failure of the mission. For this reason, hazard detection and avoidance is one of the main drivers in the design of the GNC system. A extended discussion of a Hazard Detection and Avoidance concept based in similar sensors can be found in [35]. The main function of the sensors is to perform a Hazard mapping of the landing area surroundings. The Lidars are used mainly for slope and roughness mapping (assessing the existence of rocks and out of bounds slopes through the reconstruction of a Digital Elevation Model of the terrain) and the optical cameras for shadow mappings. As a backup, the optical sensors can also perform the slope and roughness mapping.

A summary of the sensors selected is found in table 4.6. More information about the suggested sensors can be found in appendix D.

Sensor	Amount	Name	Manufacturer	Main Function
IMU	2	Miniature IMU	Honeywell	Inertial Navigation
IMU	1	LN-200S	Northrop Grumman	Inertial Navigation
Optical Camera	1	Self-designed		Mapping
Flash Lidar	1	DragonEye	ASC	Navigation, HDA
Descent Camera	1	MARDI	MSSS	Navigation, HDA
Lidar Velocimeter	1	NA	Efacec	Altimetry, Velocimetry

**Table 4.6:** Sensors for GNC and Hazard Detection and Avoidance

# Chapter 5

## Simulation, Analysis and Performance of the Landing

### 5.1 Introduction

In the past chapters, an introduction and brief explanation of the requirements needed for the mission, an analysis of the different descent strategies and a first selection of instruments for GNC have been made. In this chapter the development of a simulator to evaluate the performance of the proposed solution is explained. This simulator has been developed using the commercial software MATLAB® and its Model-Based Design tool SIMULINK.

### 5.2 Simulator Development

The simulator of the dynamics of the lander in the descent phase has been developed in two different stages. First, the different studied descent strategies have been implemented as independent Matlab scripts. The aim of that individually asses their performance and to find the individual optimal design parameters. In this first step all the relevant design parameters have been chosen and the mission scenario for the descent was finalized.

After the mission scenario was configured and the selected landing guidance laws were individually tested, the SIMULINK model was built to bring together all the individual pieces of the descent. This simulator allow us to check the interaction between the different guidance and to gradually increment the fidelity of the simulation by adding real world effects such as noisy measurements or forces disturbances in the model.

This two step approach also helped us to accommodate the quick changes that the project baseline was suffering as part of an iterative design project. Specifically and

due to the high non-linearity of the differential equations that model the descent, changes in the lander dry mass have huge impact in the design parameters of the different guidance laws. It was possible to re-evaluate and test the design parameters when changes on the baseline were made and the integrate those changes in the whole descent model.

Some of the challenges faced in the development of the simulator will be stated here.

### 5.2.1 The braking phase model

As explained in section 3.5, the descent sequence begins at the periapsis of the descent ellipse with a braking phase. The control law of this phase has been derived in section 3.4.4 so no further comments will be made. However, the challenges of implementing the control law are yet to be commented.

The first challenge to face is how to integrate the dynamics of the lander. The dynamic was ruled by the following set of equations.

$$\dot{r} = v_r \quad (5.1)$$

$$\dot{\phi} = \frac{v_\phi}{r} \quad (5.2)$$

$$\dot{v}_r = \frac{v_\phi^2}{r} - \frac{\mu_M}{r^2} + \frac{kT_{max}}{m} \sin \beta \quad (5.3)$$

$$\dot{v}_\phi = -\frac{v_r v_\phi}{r} + \frac{kT_{max}}{m} \cos \beta \quad (5.4)$$

$$\dot{m} = -\frac{kT_{max}}{I_{sp}} \quad (5.5)$$

Equations 5.1-5.5 describe a system of coupled non linear differential equations with no analytical solution. For this reason, numerical integration is needed to integrate the motion. In our case, a Runge-Kutta with adaptative step size is used. After a simple analysis, it is clear that this equations involved quantities with different magnitude orders

Distances  $\sim 10^7$  m

Angles  $\sim 1$  rad

Velocities  $\sim 10^3$  m · s<sup>-1</sup>

Mass  $\sim 10^3$  Kg

To avoid numerical integration errors in our solutions that led to wrong design parameters, it is needed to normalize the equations so all involved quantities have the same order of magnitude. The normalization parameters (identified with the superscript \*) can be derived by analysis of the natural units of the problem. For the distance, the natural unit of the problem is the Radius of the Moon.

By using radians, the order of magnitude of the angles is already the unit, so no normalization is needed. The mass is normalized with the dry mass of the lander  $m_{dry}$ . We clearly have two different orders of magnitude for the velocities. One is the transversal velocity  $v_\phi$ . This velocity is in the order of the orbital speed. Another fundamental velocity can be derived with the distance natural unit of distance  $R_M$ , mass  $m_{dry}$  and force  $T_{max}$ . This other velocity will be used for the radial velocity.

$$r^* = R_M \quad (5.6)$$

$$v_\phi^* = \sqrt{\frac{\mu_M}{R_M}} \quad (5.7)$$

$$v_r^* = \sqrt{\frac{R_M T_{max}}{m_{dry}}} \quad (5.8)$$

$$M^* = m_{dry} \quad (5.9)$$

By using the following normalized variables:

$$r_n = \frac{r}{r^*} \quad , \quad v_{r_n} = \frac{v_r}{v_r^*} \quad (5.10)$$

$$v_{\phi_n} = \frac{v_\phi}{v_\phi^*} \quad , \quad m_n = \frac{m}{M^*} \quad (5.11)$$

The normalized equations are

$$\dot{r}_n = v_{r_n} \frac{v_r^*}{r^*} \quad (5.12)$$

$$\dot{\phi} = \frac{v_{\phi_n}}{r_n} \frac{v_\phi^*}{r^*} \quad (5.13)$$

$$\dot{v}_{r_n} = \frac{v_{\phi_n}^2}{r_n} \frac{v_\phi^*}{v_r^* r^*} - \frac{\mu_M}{r_n^2} \frac{1}{r^{*2} v_r^2} + \frac{k_{max} T_{max}}{m_n} \sin \beta \frac{1}{v_r^* M^*} \quad (5.14)$$

$$\dot{v}_{\phi_n} = - \frac{v_{r_n} v_{\phi_n}}{r_n} \frac{v_r^*}{r^*} + \frac{k_{max} T_{max}}{m_n} \cos \beta \frac{1}{v_\phi^* M^*} \quad (5.15)$$

$$\dot{m}_n = - \frac{k_{max} T_{max}}{m_n I_{sp}} \quad (5.16)$$

This new set of equations can be easily integrated numerically with the proposed integration scheme.

Choosing the two adequate initial costate values  $\mathbf{p}_0$  to achieve the desired final position and velocity is a complex mathematical problem with no close solution. To solve it, it is treated as a separate optimization subproblem. We want to pick the two values of the costates initial values that minimizes the following functional  $\Upsilon$

$$\Upsilon(\mathbf{p}_0) = [\mathbf{r}(tf) - \mathbf{r}_d]^T [\mathbf{r}(tf) - \mathbf{r}_d] + [\mathbf{v}(tf) - \mathbf{v}_d]^T [\mathbf{v}(tf) - \mathbf{v}_d] \quad (5.17)$$

This functional achieves its minimum when the final position and velocity are the desired ones. Due to the characteristics of the equations involved, usual optimization solving techniques such as conjugated gradient cannot be used to solve it. However, iterative methods as genetic algorithms and random search have quick convergence rates when adequate boundaries are given. In this case, a controlled random search [36] has been implemented. This random search only has to be run once to find the two design parameters of the algorithm and does not have to occur in real time. It can be run before the descent begins in case we want to change the braking phase nominal trajectory.

The end altitude for this algorithm has been established as 4 km. At this point, the flash lidar camera begins to operate, providing us with more accurate measures of velocity and position. At this point the approach phase begins.

### 5.2.2 Approach Phase

In the approach phase the ZEM/ZEV guidance law is used. As we have already removed all the orbital velocity and we are close to the landing site the optimal trajectories generated does not include subsurface flight sequence. There is no need now to use the Model Predictive Static Programming, that requires extra computational effort. The whole guidance can be controlled and optimized by selecting the adequate value of the total manoeuvre duration. As the control only depends on the ZEM/ZEV quantities, fixed by the dynamics, and the  $t_{go}$ , this last parameter could be optimized at each step to accommodate any disturbance that affects the dynamics. As the manoeuvre only depends of one design parameter, a simple line search can be used for optimization. This adaptive  $t_{go}$  has not been implemented in the simulator and the total duration of the manoeuvre is selected at the beginning by using the mentioned line search technique. This could be implemented in further developments of the simulator.

As we are in the vicinity of the landing site at an altitude of 4 km or less with most of the orbital velocity removed, the following simplifications on the dynamic model can be made

- Flat Moon assumption. The effect of the curvature of the Moon can be neglected.
- Constant gravity. The gravity vector has a constant value and fixed vertical direction.
- A 3D model with topocentric Cartesian axis centred in the landing site will be used to asses the full re-targetting capabilities .

- The reference frame is orientated with the Z axis in the vertical direction, X in the horizontal projection of the lander's velocity and Y forming a right hand side set.

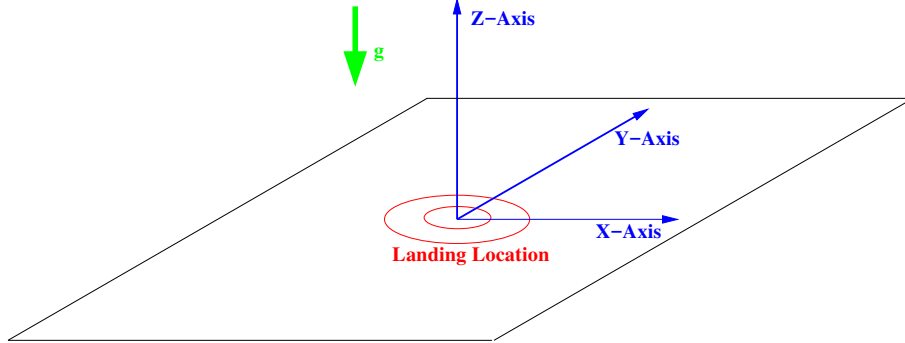


**Figure 5.1:** New reference system for the descent

The differential equations of the new model are:

$$\dot{x} = v_x \quad (5.18)$$

$$\dot{y} = v_y \quad (5.19)$$

$$\dot{z} = v_z \quad (5.20)$$

$$\dot{v}_x = a_x = \frac{T_x}{m} \quad (5.21)$$

$$\dot{v}_y = a_y = \frac{T_y}{m} \quad (5.22)$$

$$\dot{v}_z = a_z - g_M = \frac{T_z}{m} - g_M \quad (5.23)$$

$$\dot{m} = \frac{\sqrt{T_x^2 + T_y^2 + T_z^2}}{I_{sp}} \quad (5.24)$$

$$(5.25)$$

$$k_{min}T_{max} \leq \sqrt{T_x^2 + T_y^2 + T_z^2} \leq k_{max}T_{max} \quad (5.26)$$

This new set of differential equations is easier to integrate and does not require any normalization for acceptable performance.

The ZEM/ZEV algorithm directly produces the acceleration commands  $a_x, a_y, a_z$ . This commands can be easily translated into attitude and throttle commands

$$\begin{Bmatrix} a_x \\ a_y \\ a_z \end{Bmatrix} = \frac{k}{m} \begin{Bmatrix} \hat{u}_x \\ \hat{u}_y \\ \hat{u}_z \end{Bmatrix} = \frac{k}{m} \hat{\mathbf{u}} \quad (5.27)$$

where  $\hat{\mathbf{u}}$  is the attitude unity vector in the reference frame.

This descent phase ends with the lander vertically hovering 100 m over the landing site with a vertical velocity of  $-5 \text{ m}\cdot\text{s}^{-1}$ .

### 5.2.3 Vertical Descent

In this phase, the same reference frame and dynamic equations as the approach phase are used. The only change is the guidance law. The thrust level of the engine is calculated to counteract the weight of lander, achieving a constant velocity descent. At this the Hazard Detection and Avoidance Algorithm would assure a successful landing in a Hazard free area. Horizontal displacement and fine positioning can be achieved using the reaction control thrusters.

## 5.3 The descent and landing simulator

The following step was to merge all the developed MATLAB® scripts into a single SIMULINK Model. A caption of this model is shown in figure

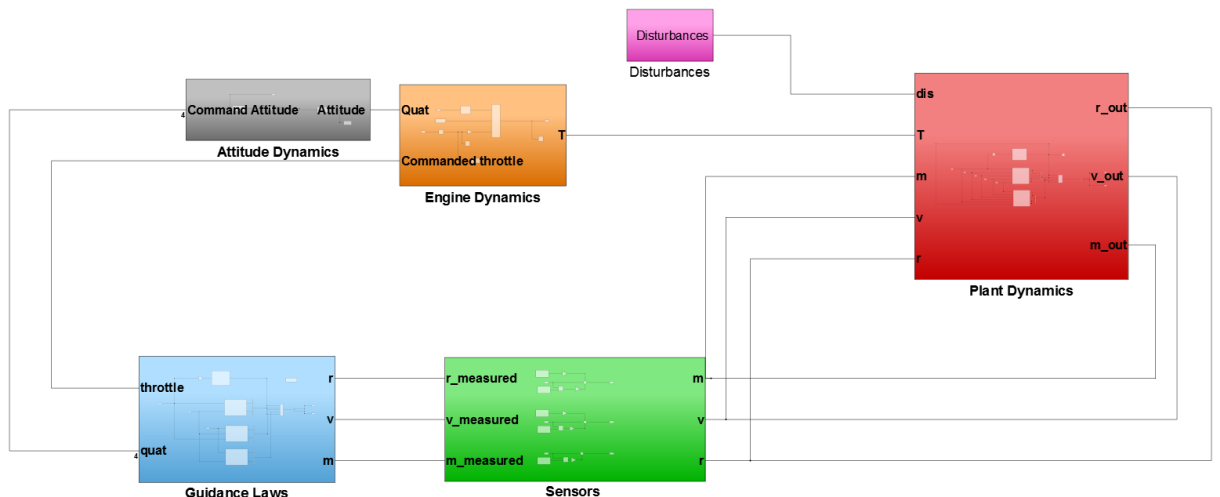


**Figure 5.2:** Overview of the descent simulator

It can be shown how the model is divided in 6 main blocks. A brief explanation of these blocks will be given now.

### 5.3.1 Plant Dynamics

The red block is the plant dynamics. This block simulates the motion of the lander in the Lunar environment using the equations derived before. It is important to use the right set of equations at each phase of the descent. For the braking phase, the full 3D model is used now instead of the simpler 2D model used for deriving the guidance laws. For this reason, a custom phase selector block computes the altitude above the landing site to chose the correct plant dynamics. It is also critical to make sure that the axis transformations between the different references systems are made correctly.

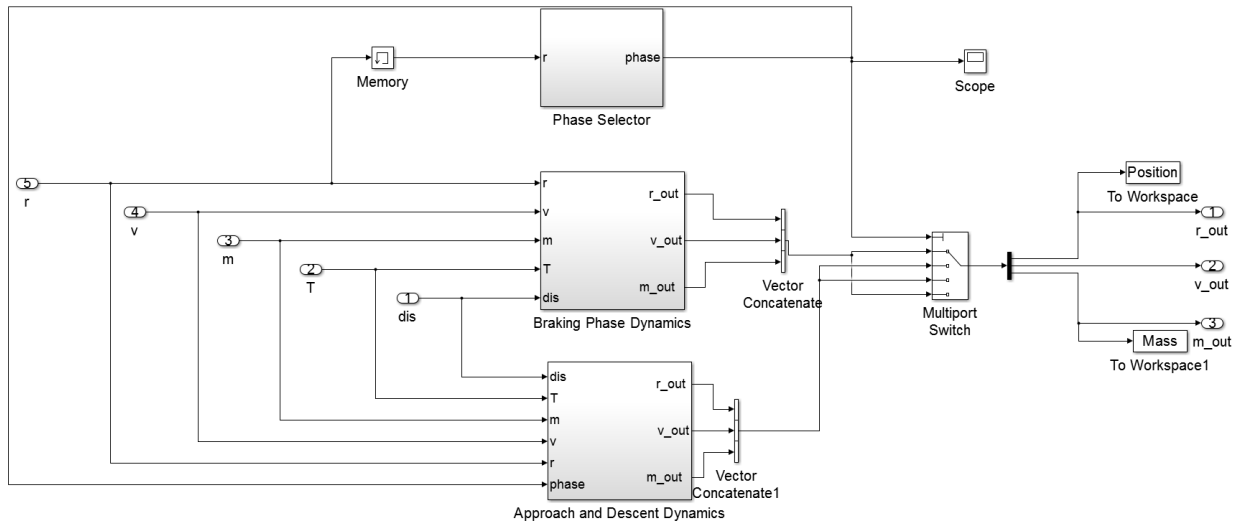


**Figure 5.3:** Plant Dynamics

### 5.3.2 Sensors

The green box simulates the sensor measurements as they would come out from the Kalman filter. The actual Kalman filter has not been implemented. To simulate real-measures, to the state vector generated by the plant dynamics (position, velocity and mass) normal distributed noise is added. This noise measures are the one fed into the guidance algorithms instead of the lander true position, velocity and mass as would occur in a real implementation.

### 5.3.3 Guidance laws

With a similar construction as the plant dynamics. This block evaluates the phase of the descent sequence by computing the altitude relative to the landing site. After that, the relevant control command is fed to the attitude and engine dynamics blocks.

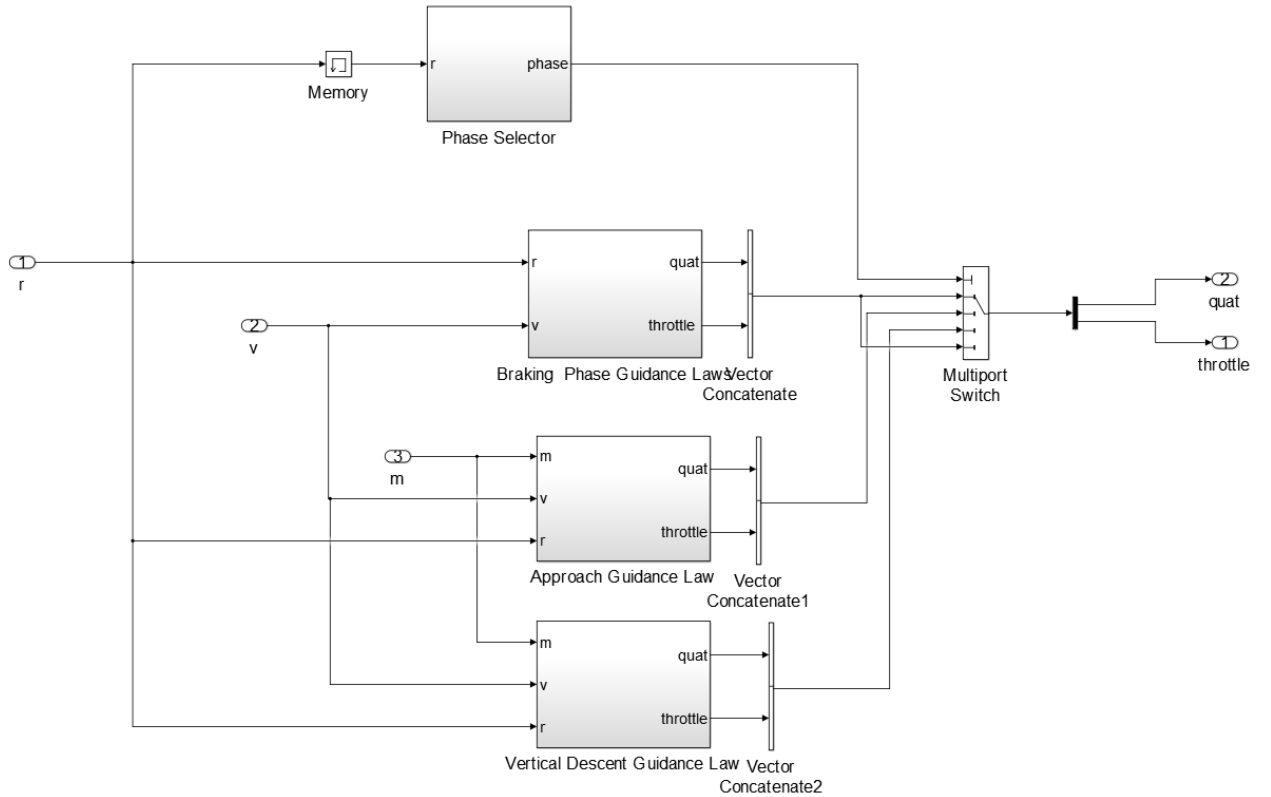


**Figure 5.4:** Guidance laws

### 5.3.4 Attitude Dynamics and Engine Dynamics

In this blocks, it is checked if the commanded attitude and throttle of the guidance laws can be achieved. At this point of the project, the attitude controller of the AOCS WP [12] had not been developed so the attitude block only checks for if the attitude rate of change between two consecutive commands falls below the maximum angular velocity value provided by the AOCS WP. The engine dynamics block also limits the values of the throttle so they lie between the established maximum and minimum and it converts the throttle position and achieved attitude into three forces in each of the axis of the reference frame.

### 5.3.5 Disturbances

The last block accounts for any possible disturbance that can affect the dynamics of the lander. Those disturbances can be attitude control failures, thrust misalignments, external perturbations and, in general, any other action that has not been taken into account in the modelling. This disturbances, in conjunction with serve to generate the landing ellipse using the Montecarlo method.

## 5.4 Analysis of the results

In this section, the results from the simulator will be shown and analysed. First, the nominal trajectory, the trajectory that the lander would follow in an ideal situation with no disturbances acting on it will be presented. Then the performance of a realistic case will be analysed using the Montecarlo method.

### 5.4.1 Nominal Descent Trajectory

In the nominal descent, the following assumptions are true

- No disturbances act on the lander.
- The sensors know the true position, velocity and mass at each step of integration.
- Due to the reference frames defined, all the trajectory is 2D.

In figure 5.5 the nominal trajectory followed by the lander is shown with different colors for the three phases. Most of the trajectory corresponds with the braking phase. A closer detail of the final part with the approach and descent phases is shown in figure 5.6.

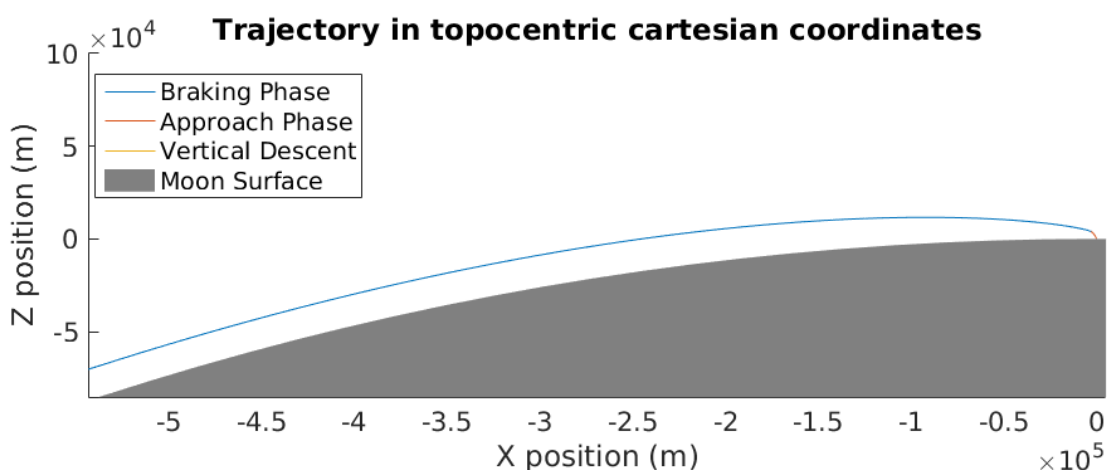


**Figure 5.5:** Nominal trajectory in topocentric axes for the descent

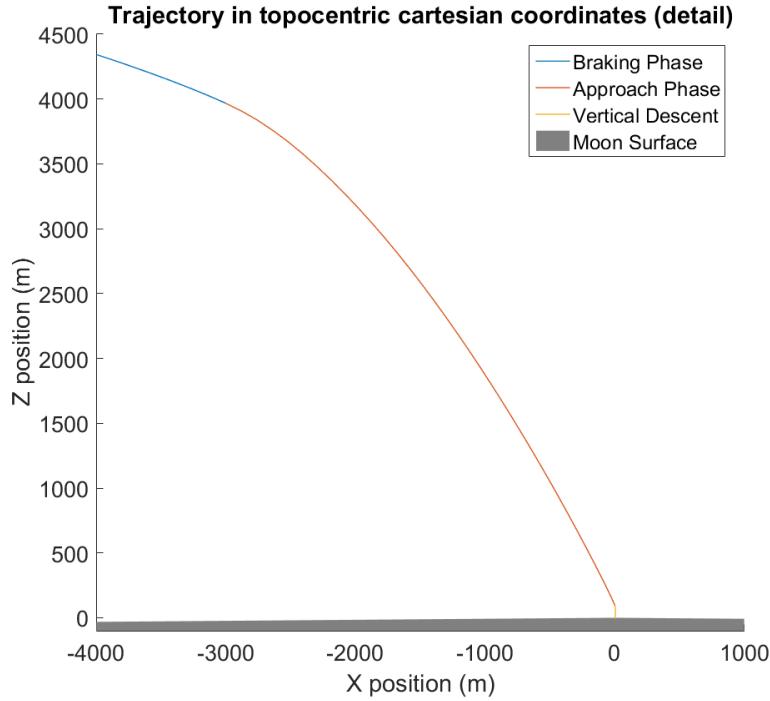


**Figure 5.6:** Detail of nominal trajectory in topocentric axes for the descent

In figure 5.7, the altitude of the lander versus the time is plot. The threshold altitudes of 4 km and 100, where the guidance law is changed are also shown.

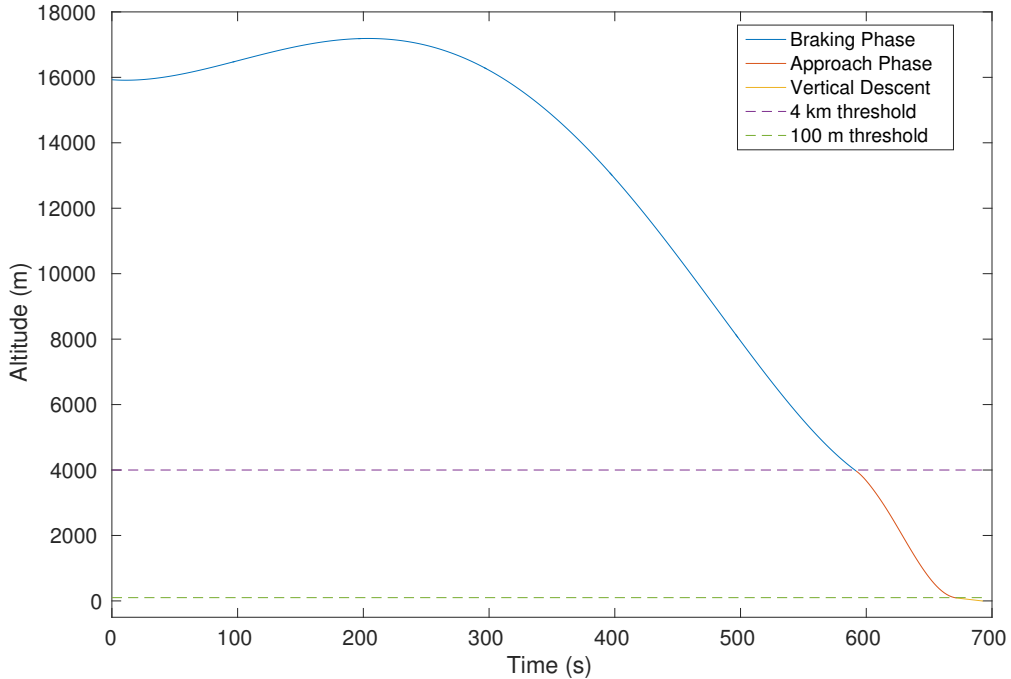


**Figure 5.7:** Nominal altitude profile for the descent

In figure 5.8 the velocity profile in all three axis is shown. As the nominal trajectory without disturbances is purely 2D trajectory, the values in the Y axis are 0.

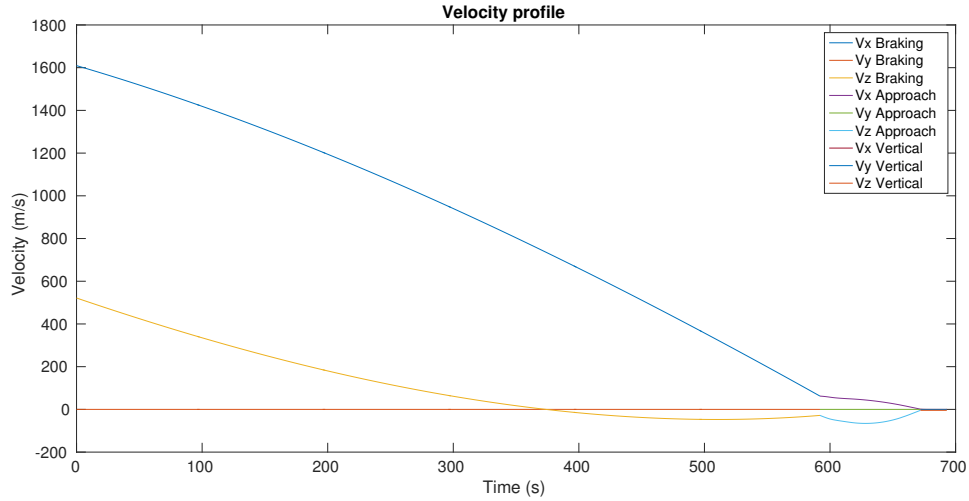


**Figure 5.8:** Nominal velocity profile for the descent

In the following figure, the evolution of the lander mass is presented. The propellant mass consumption rate is constant in the initial braking phase, as the engines are fired at full throttle.

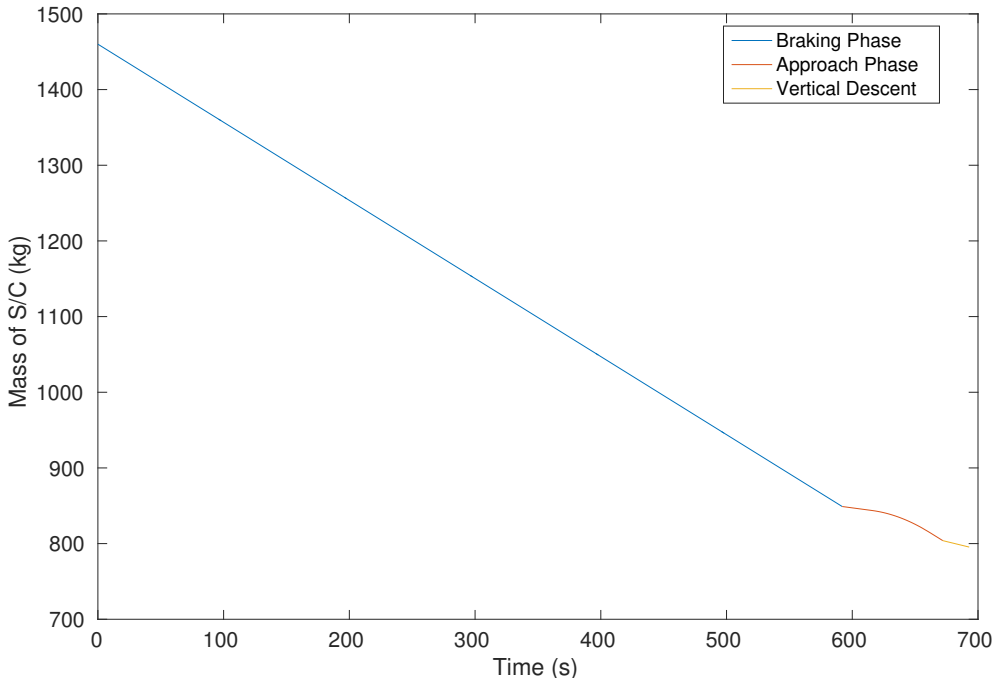


**Figure 5.9:** Nominal mass profile for the descent

Finally, the throttle command  $k$  during the whole descent is shown in figure 5.10. As stated before the throttle is maximum in the braking phase, is then continuously controlled in the approach phase and it is almost constant in the final vertical descent phase, as the mass changes in that phase are minimum.

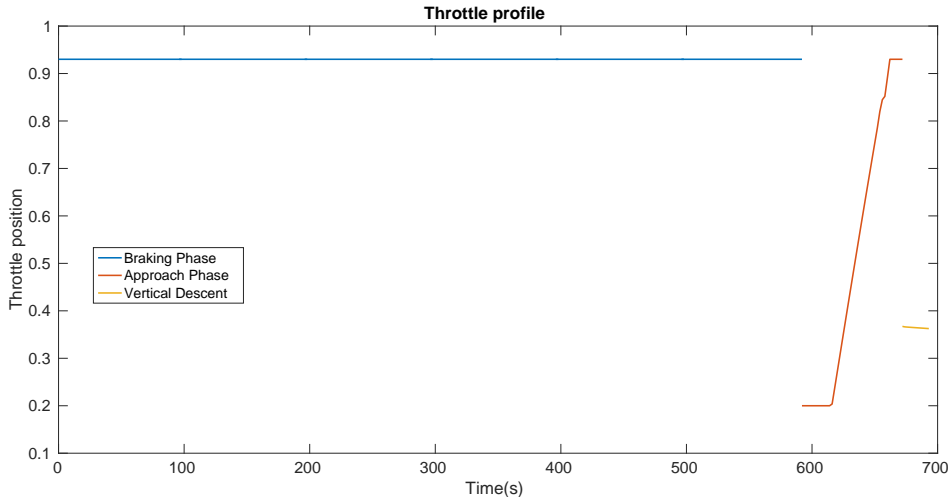


**Figure 5.10:** Nominal throttle profile for the descent

The relevant characteristics of each phase of the descent sequence are shown in table 5.1 with a 10% included in the mass.

Phase	Braking	Approach	Vertical Descent
<b>Lander Mass at beginning</b>	1460 kg	849 kg	809 kg
<b>Lander Mass at end</b>	849 kg	804 kg	797 kg
<b>Altitude at beginning</b>	15000 m	3966 m	98.4 m
<b>Altitude at end</b>	3966 m	98.4 m	0 m
<b>Downrange at beginning</b>	543360 m	3000 m	0 m
<b>Downrange at end</b>	3000 m	0 m	0 m
<b>Duration</b>	592 s	82 s	17 s
<b>Propellant Mass</b>	611 kg	45 kg	7 kg
<b><math>\Delta V</math></b>	$1739 \text{ m}\cdot\text{s}^{-1}$	$173 \text{ m}\cdot\text{s}^{-1}$	$27 \text{ m}\cdot\text{s}^{-1}$

**Table 5.1:** Parameters of the descent phases

A summary of the relevant budgets for the descent and landing is shown in table 5.2.

Total	
<b>Duration</b>	691 s
<b>Propellant</b>	663 kg
<b><math>\Delta V</math></b>	$1939 \text{ m}\cdot\text{s}^{-1}$

**Table 5.2:** Budgets for descent and landing

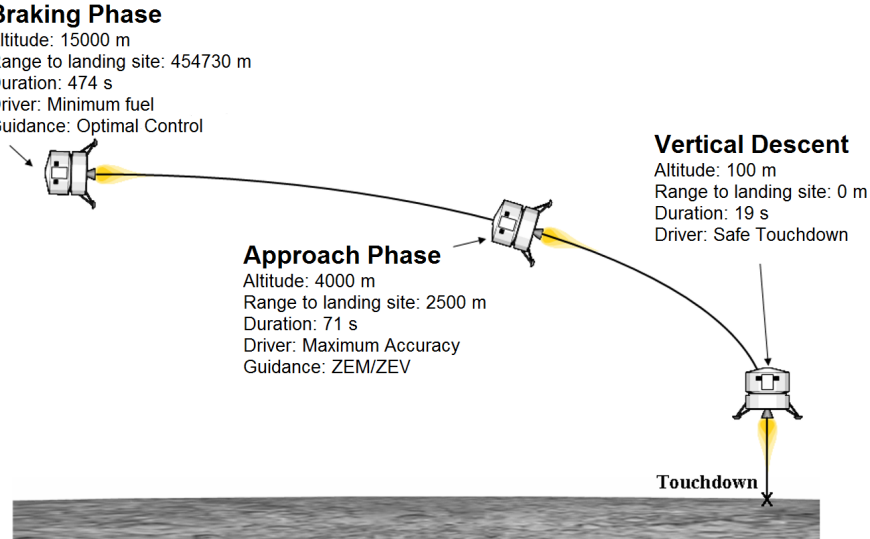


**Figure 5.11:** Summary of the nominal descent sequence

### 5.4.2 Performance of the algorithms

After the analysis of the nominal descent sequence, we want to simulate a more realistic implementation of our guidance laws. The simulator developed in SIMULINK incorporates the real implementation effect through the noise in the sensors and the disturbances. The noise measures affect the position, velocity and mass used to compute the control commands. The disturbances are modelled as extra forces acting on the lander. Both of this effects are modelled using a normal distribution with zero mean and different values of standard deviation

To evaluate the performance of the proposed algorithm, the Montecarlo method has been used. 1000 simulations were carried out to compute the landing ellipse. Due to the use of inertial navigation (the position is known by double integration of the acceleration and the velocity by a single integration of the acceleration) , it is expected that the biggest errors appear in the position measures and not in the velocities. No great error are expected in the mass values, as the propellant flow can be easily measured on board, only a 2% error of the actual mass was considered. The disturbances will have to account for any uncertainty of the model as, for example, the lack of the definitive attitude controller, as well as for any possible operation failures such as thrust misalignments. For this reason, the standard deviation of the disturbances has been set to a high value which is the 20% of the total thrust of the propulsion system.

The standard deviations used in the normal distributed noise and disturbances are shown in table 5.3.

Standard Deviations $\sigma$	
Position	5000 m
Velocity	$50 \text{ m}\cdot\text{s}^{-1}$
Mass	2%
Force disturbances	$0.2T_{max} = 712 \text{ N}$

**Table 5.3:** Montecarlo Simulation Parameters

With this mentioned values the landing ellipse has been calculated and it is plot in figure 5.12.

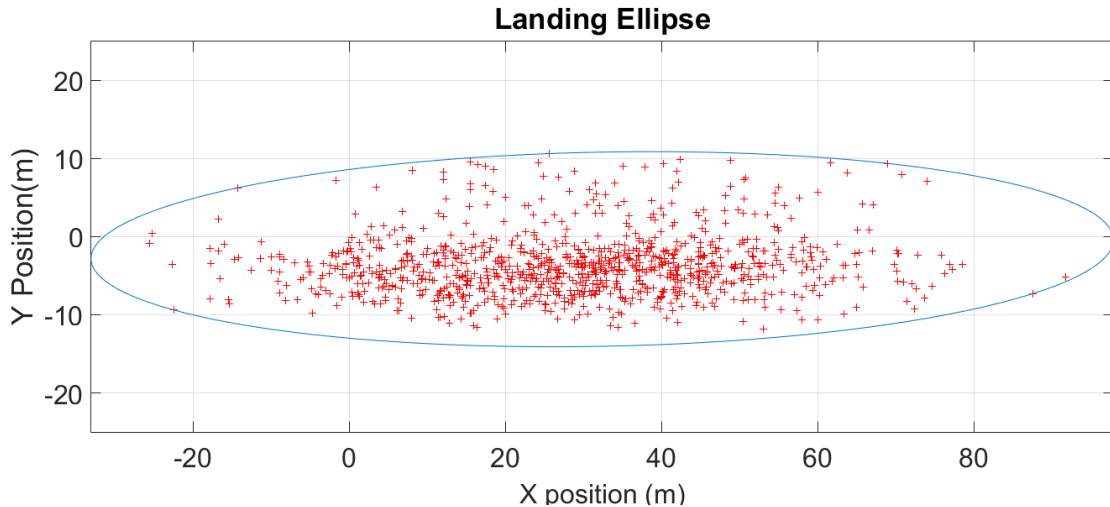


**Figure 5.12:** Landing ellipse of the mission computed with 1000 simulations

The landing ellipse is the main Figure of Merit that allow us to asses the performance of the algorithms. It can be seen how the main requirement of the descent and landing **R\_DL\_05** *The spacecraft shall be able to land inside a 200x200 m landing ellipse centred in the landing site* has been completely fulfilled. This have been achieved minimizing the propellant mass consumption while retaining the re-targeting capabilities needed for the Hazard Detection and Avoidance algorithms.

While for the nominal descent sequence the spacecraft landed mass was considered to be 800 kg this value is not exactly the final dry mass of the lander. As stated in appendix B the spacecraft landed mass is 745 kg. The extra 50 kg of contingency propellant account for extra manoeuvres required for the Hazard Detection and Avoidance algorithms. With those extra 50 kg, it is possible to move the lander up to 10 km from the nominal landing site.

# Chapter 6

## Conclusions and future work

### 6.1 Conclusions

Through this document, a complete analysis of the descent and landing work package of the Lunar Mission One has been carried out. The top level requirements have been derived from the Mission Statement and from further analysis in chapter 2. The main drivers for the design of the descent sequence were found to achieving high accuracy while minimizing the propellant consumption and allowing landing site re-targeting. In 3 different proposed soft landing strategies were studied and two of them were selected for the design of the final descent sequence. This descent sequence was divided in three different phases: a braking phase, an approach phase and a vertical descent phase. After that, in chapter 4, a selection of instruments for the descent were suggested. This selection of instruments consists in 4 main engines, two optical cameras (mapping camera and descent camera), two Lidar sensors (flash Lidar camera and Lidar Velocimeter) and three inertial measurement units. The integration of all this sensors into a general GNC scheme has been briefly outlined. Finally, a simulator of the dynamics of the lander were developed using MATLAB® and its performance was assessed through the calculation of the landing ellipse. This evaluation showed that all the requirements derived in 3 can be met by the proposed configuration.

We can conclude that all the objectives established at the beginning of this project for the Descent & Landing Work Package and outlined in 1.2 have been fulfilled.

## 6.2 Future Work

If the project were to continue the natural next steps would be focused on improve the simulator to have a better representation of the real implementation. Some of those next steps are briefly outlined here

1. Research and implementation of the Hazard Detection and Avoidance Algorithms.
2. Implementation of the attitude controller of the AOCS WP.
3. Improve the model of the different measures of the proposed sensors.
4. Implementation of the Kalman filtering estimation techniques.

# References

- [1] Diego De Rosa, Ben Bussey, Joshua T. Cahill, Tobias Lutz, Ian A. Crawford, Terence Hackwill, Stephan Van Gasselt, Gerhard Neukum, Lars Witte, Andy McGovern, Peter M. Grindrod, and James D. Carpenter. Characterisation of potential landing sites for the European Space Agency’s Lunar Lander project. *Planetary and Space Science*, 74(1):224–246, 2012.
- [2] M Anand, I A Crawford, M R Sims, A Smith, R Burgess, K H Joy, C S Cockwell, M A Sephton, S S Russel, C L Smith, Smith D J, G Woan, N Bowles, M M Grady, J C Zarnecki, and D Iron. Lunar Mission One: The first Crowdfunded Mission to the Moon Presenting New Opportunities for Lunar Science. In *46th Lunar and Planetary Science Conference*, pages 8–9, 2015.
- [3] Ian Andrew Crawford, Mark Sims, Alan Smith, Mahesh Anand, Neil Bowles, Ray Burgess, Charles Cockell, Katherine Joy, Mark Sephton, Sara Russell, David E. Smith, Graham Woan, and John Zarnecki. Preliminary Lunar Science Drivers for Lunar Mission One. Technical Report December, 2014.
- [4] Roland Albers. LM1: Project Management, Requirements and Structures. Technical report, Cranfield University, Cranfield, 2016.
- [5] D B J Bussey, J A McGovern, P D Spudis, C D Neish, H Noda, Y Ishihara, and S Sørensen. Illumination conditions of the south pole of the Moon derived using Kaguya topography. *Icarus*, 208(2):558–564, 2010.
- [6] Benjamin Vanoutryve, Diego De Rosa, Richard Fisackerly, Berengere Houdou, James Carpenter, Christian Philippe, Alain Pradier, Aliac Jojaghaian, Sylvie Espinasse, and Bruno Gardini. An analysis of illumination and communication conditions near Lunar South Pole based on Kaguya data. Technical report, European Space Agency, Noordwijk.
- [7] Paul D. Spudis, Ben Bussey, Jeffrey Plescia, Jean Luc Joset, and St??phane Beauvivre. Geology of Shackleton Crater and the south pole of the Moon. *Geophysical Research Letters*, 35(14):0–4, 2008.
- [8] Alisa Michelle Hawkins. Constrained Trajectory Optimization of a Soft Lunar Landing from a Parking Orbit. (2003), 2005.
- [9] Zoé Tenacci. Lunar Mission One - Operations. Technical report, Cranfield University, Cranfield, 2016.

- [10] Alan W Wilhite, John Wagner, Robert Tolson, and Marina Mazur Moen. Lunar Module Descent Mission Design. *AIAA/AAS Astrodynamics Specialist Conference and Exhibit*, (August), 2008.
- [11] Daniel Grinham. Lunar Mission One: Trajectory Design and Analysis. Technical report, Cranfield University, Cranfield, 2016.
- [12] Jean Michael Irock. Lunar Mission One: Attitude & Orbit Control Subsystem. Technical report, 2016.
- [13] Bong Gyun Park and Min Jea Tahk. Three-dimensional trajectory optimization of soft lunar landings from the parking orbit with considerations of the landing site. *International Journal of Control, Automation and Systems*, 9(6):1164–1172, 2011.
- [14] I. Michael Ross and Fariba Fahroo. Pseudospectral Knotting Methods for Solving Nonsmooth Optimal Control Problems. *Journal of Guidance, Control, and Dynamics*, 27(3):397–405, 2004.
- [15] Allan R. Klumpp. Apollo lunar descent guidance. *Automatica*, 10(2):133–146, 1974.
- [16] Paul Zarchan. *Tactical and Strategic missile guidance.pdf*. American Institute of Aeronautics and Astronautics, Inc., Atlanta, 1994.
- [17] Liuyu Zhou and Yuanqing Xia. Improved ZEM/ZEV feedback guidance for Mars powered descent phase. *Advances in Space Research*, 54(11):2446–2455, 2014.
- [18] Matt Hawkins. *New near-optimal feedback guidance algorithms for space missions*. PhD thesis, Iowa State University, 2013.
- [19] Daniel R. Wibben and Roberto Furfaro. Optimal sliding guidance algorithm for Mars powered descent phase. *Advances in Space Research*, 57(4):948–961, 2016.
- [20] Yanning Guo, Matt Hawkins, and Bong Wie. Applications of generalized zero-effort-miss / zero-effort-velocity feedback guidance algorithm. *Advances in the Astronautical Sciences*, 143(3):1403–1422, 2012.
- [21] Bo Zhang, Shuo Tang, and Binfeng Pan. Multi-constrained suboptimal powered descent guidance for lunar pinpoint soft landing. *Aerospace Science and Technology*, 48:203–213, 2016.
- [22] Matthew J. Casiano, James R. Hulka, and Vigor Yang. Liquid-Propellant Rocket Engine Throttling: A Comprehensive Review. *Journal of Propulsion and Power*, 26(5):897–923, 2010.
- [23] H Flugge-Lotz, I; Halkin. Pontryagin’s maximum principle and optimal Control. Technical report, Stanford University. Division of Engineering Mechanics, Stanford, 1961.

- [24] David Vallado. *Fundamentals of Astrodynamics and applications*. Microcosm Press, Hawthorne, 4th edition.
- [25] Jeremy R Rea and Robert H Bishop. Analytical Dimensional Reduction of a Fuel Optimal Powered Descent Subproblem. *Current*, pages 1–32.
- [26] G A Dressler. Summary of Deep Throttling Rocket Engines with Emphasis on Apollo LMDE. *AIAA/ASME/SAE/ASEE Joint Propulsion Conference & Exhibit*, 42(July):19, 2006.
- [27] Carl Stechman and Steve Harper. Performance Improvements in Small Earth Storable Rocket Engines- An Era of Approaching the Theoretical. *46th AIAA/ASME/SAE/ASEE Joint Propulsion Conference & Exhibit*, (July):1–11, 2010.
- [28] James R Wertz. *Space Mission Engineering: The New SMAD*. Microcosm Press, Hawthorne, 2015.
- [29] C Keller, H U; Barbieri, H; ; Lamy, P, Rickman, R; Wenzel K P; Rodrigo, and H Sierks. OSIRIS - The scientific camera system onboard Rosetta. *Space Science Reviews*, 128(1-4):433–506, 2007.
- [30] Baochang Zhao, Jianfeng Yang, Desheng Wen, Wei Gao, Lingying Chang, Zongxi Song, Bin Xue, and Wei Zhao. Overall scheme and on-orbit images of Chang'E-2 lunar satellite CCD stereo camera. *Science China Technological Sciences*, 54(9):2237–2242, 2011.
- [31] M C Malin, James F Bell, and J Cameron. The mast cameras and Mars Descent Imager (MARDI) for the 2009 Mars Science Laboratory. *Lunar and Planetary Science*, 36(2005):4–5, 2005.
- [32] Jean de Lafontaine, Arkady Ulitsky, Jeffrey W. Tripp, Robert Richards, Michael Daly, and Christian Sallaberger. LAPS: the development of a scanning lidar system with GNC for autonomous hazard avoidance and precision landing. 5418:81–93, 2004.
- [33] Andres Huertas, Andrew E. Johnson, Robert A. Werner, and Robert A. Maddock. Performance evaluation of hazard detection and avoidance algorithms for safe lunar landings. *IEEE Aerospace Conference Proceedings*, 2010.
- [34] Mohamad Aqeel Shamsul Anuar. LM1: Lunar Mission One baseline and configuration. Technical report, Cranfield University, Cranfield, 2016.
- [35] Baltazar Parreira, José F. Vasconcelos, Javier Montaño, Jose Ramón, and Luis F Penin. Hazard Detection and Avoidance in ESA Lunar Lander: Concept and Performance. *To be presented at AIAA Guidance, Navigation and Control Conference*, pages 1–12, 2013.
- [36] R. V. Ramanan and Madan Lal. Analysis of optimal strategies for soft landing on the moon from lunar parking orbits. *Journal of Earth System Science*, 114(6):807–813, 2005.

- [37] Dale Wyllie. Lunar Mission One - Launch and Surface Penetrators. Technical report, Cranfield University, Cranfield, 2016.
- [38] Oscar Rodriguez Fernandez. Lunar Mission One: Descent & Landing. Technical report, Cranfield University, Cranfield, 2016.
- [39] Daniel Hadfield. Lunar Mission One - Scientific Payload & OBDH. Technical report, Cranfield University, Cranfield, 2016.



# Appendix A

## Executive Summary: LMO - Descent & Landing

In this appendix the relevant facts and figures of the descent and landing work package are summarized.

### A.1 Requirements

For the descent & landing work packages, the top-level requirements are:

- R\_DL\_01** The spacecraft shall be able to land on the Lunar South Pole.
- R\_DL\_02** The spacecraft shall be able to withstand the landing conditions.
- R\_DL\_03** The spacecraft shall land vertically.
- R\_DL\_04** The spacecraft shall be able to land autonomously.
- R\_DL\_05** The spacecraft shall be able to land inside a 200x200 m landing ellipse centred in the landing site.
- R\_DL\_06** The spacecraft shall be able perform an initial mapping of the potential landing sites previous to landing.
- R\_DL\_07** The spacecraft shall be able to change the landing location at any point prior or during the landing sequence.
- R\_DL\_08** The spacecraft shall be able to communicate directly with Earth during the whole landing sequence.
- R\_DL\_09** The engines of the spacecraft shall not be turned off at any point of the descent trajectory.

## A.2 Mission Scenario

From the arrival at the Moon until the landing at the designed location, the mission scenario will follow the following sequences:

1. Arrival at the Moon in an elliptical 100x15 km altitude mapping orbit. Initial mapping of the potential landing sites will be performed here.
2. Circular Parking orbit of 100 km during a whole revolution of the Moon to obtain the same geometric conditions as in the mapping.
3. Elliptical 100x15 km descent orbit.
4. At the periapsis of the orbit, beginning of the braking phase using optimal control theory as a guidance law.
5. At 4 km of altitude above the surface of the Moon, change into a Zero-Effort-Miss/Zero-Velocity-Miss guidance algorithm to begin the approach phase.
6. The approach phase finishes with the spacecraft hoovering vertically at 100 m over the landing site. A constant velocity descent places the spacecraft on the ground. Horizontal displacement achieved using reaction control thrusters.

## A.3 Mapping Camera

To assure a successful mission, a previous mapping of potential landing sites have to be carried out. An optical mapping camera able to acquire 2.5 m resolution images in swath width of 10 is designed. The relevant parameters of this imager sensor are:

Parameters	Value	Units
Focal length	331	mm
FOV	38.96	deg
Operating Wavelength	540	nm
Mass	1.15	kg
Power	28.4	W
Dimensions	127x89.2x122	mm

**Table A.1:** Mapping Camera Parameters

## A.4 Hardware for Descent & Landing

The following scheme is proposed for the Guidance Navigation and Control of the descent.

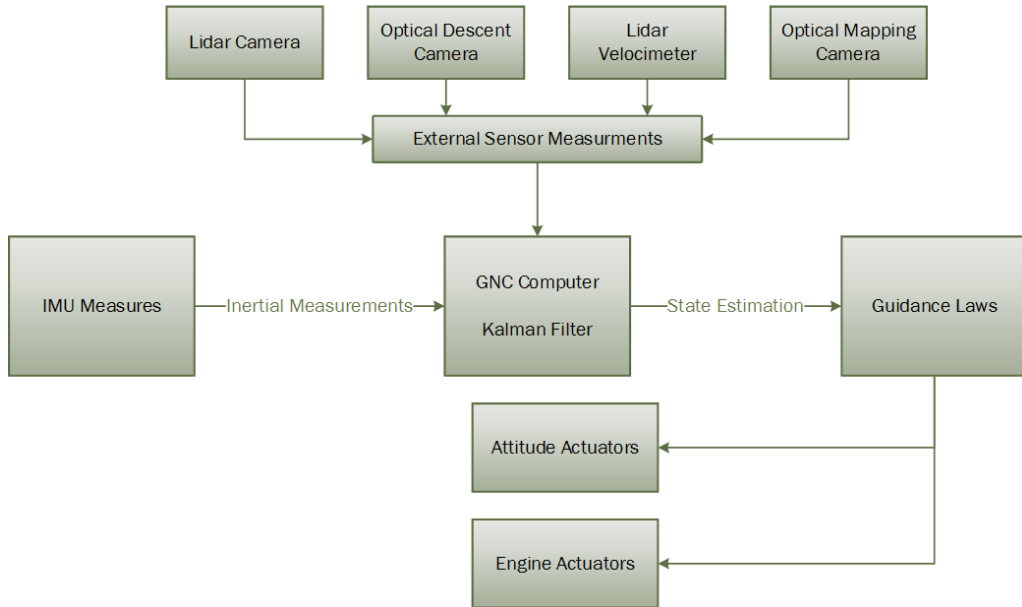


**Figure A.1:** Proposed GNC scheme for the descent

This GNC scheme will be formed by:

Component	Amount	Name	Manufacturer	Main Function
Main Engine	4	R-42DM	Aerojet	Propulsion System
IMU	2	Miniature IMU	Honeywell	Inertial Navigation
IMU	1	LN-200S	Northrop Grumman	Inertial Navigation
Optical Camera	1	Self-designed		Mapping
Flash Lidar	1	DragonEye	ASC	Navigation, HDA
Descent Camera	1	MARDI	MSSS	Navigation, HDA
Lidar Velocimeter	1	NA	Efacec	Altimetry, Velocimetry

**Table A.2:** Hardware for Descent and Landing

## A.5 Descent Sequence

The descent sequence begins at the periapsis of the landing ellipse and finishes with the spacecraft achieving a soft landing on the desired landing location. The relevant parameters of the sequence are shown in table A.3

Phase	Braking	Approach	Vertical Descent
<b>Lander Mass at beginning</b>	1460 kg	849 kg	809 kg
<b>Lander Mass at end</b>	849 kg	804 kg	797 kg
<b>Altitude at beginning</b>	15000 m	3966 m	98.4 m
<b>Altitude at end</b>	3966 m	98.4 m	0 m
<b>Downrange at beginning</b>	543360 m	3000 m	0 m
<b>Downrange at end</b>	3000 m	0 m	0 m
<b>Duration</b>	592 s	82 s	17 s
<b>Propellant Mass</b>	611 kg	45 kg	7 kg
<b><math>\Delta V</math></b>	$1739 \text{ m}\cdot\text{s}^{-1}$	$173 \text{ m}\cdot\text{s}^{-1}$	$27 \text{ m}\cdot\text{s}^{-1}$
<b>Total Duration</b>			<b>691 s</b>
<b>Total Propellant</b>			<b>663 kg</b>
<b>Total <math>\Delta V</math></b>			<b><math>1939 \text{ m}\cdot\text{s}^{-1}</math></b>

Table A.3: Parameters of the descent phases

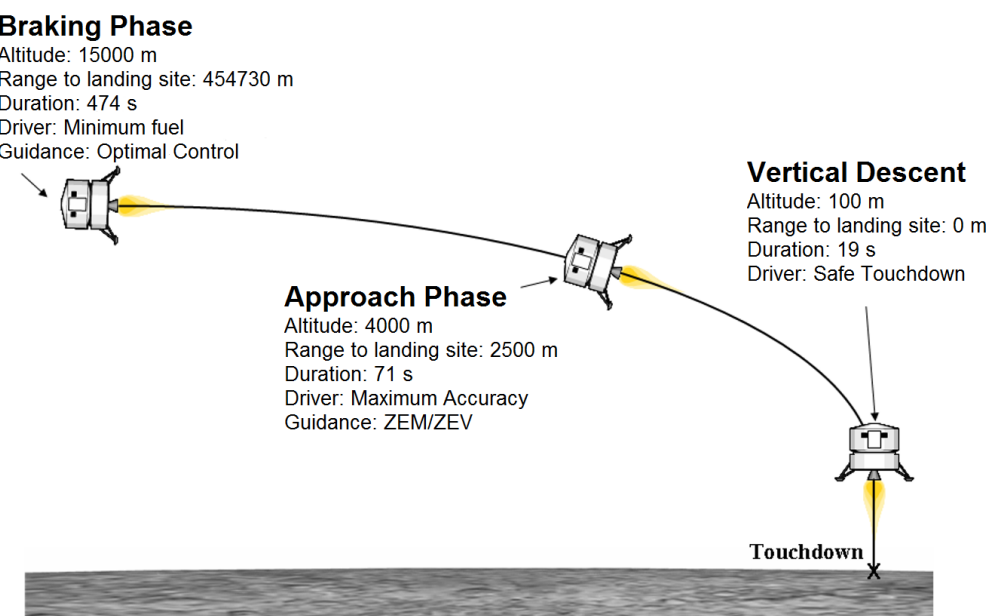


Figure A.2: Summary of the nominal descent sequence

# Appendix B

## Common Appendix

### B.1 Mission Statement

“To design a spacecraft that is able to land and drill on the lunar surface before 2024, deposit a time capsule and perform in situ scientific experiments for the purpose of future scientific exploitation and human exploration within the budget of \$0.75 Bn.”

### B.2 System Requirements

#### 1. External System interfaces

1. The spacecraft shall be able to communicate directly with a ground station.
2. The spacecraft shall have a drill capable of penetrating the lunar regolith.
3. The spacecraft shall be compatible with currently available launchers.

#### 2. Environment

1. The spacecraft shall be able to withstand Temperature swings from 100 K to 360 K,
2. The Spacecraft shall be able to withstand a continuous night of 27.7 hours.
3. The spacecraft shall be able to withstand the radiation environment during solar maxima.
4. The spacecraft shall be able to withstand launch conditions of the Falcon 9.1 launcher.

### 3. Mission, Operations, Lifetime

1. The spacecraft shall be able to perform lunar insertion, orbital manoeuvres and a powered landing.
2. The spacecraft shall land at the Shackleton Rim (site A.2) with coordinates (lat/long) - 89.7788, -153.4349 degrees.
3. The spacecraft shall be able to perform imaging of the landing site prior to descent.
4. The spacecraft shall have a minimum lifetime equivalent to the time needed to complete the drilling.
5. The spacecraft shall incorporate the necessary instrumentation to:
  - Determine existence of volatiles and their origin.
  - Investigate geochemistry/mineralogy of the lunar crust
  - Constrain model of lunar interior.
  - Characterise lunar environment for future human exploration

### 4. Functional requirements

1. The Spacecraft shall be able to drill to a minimum depth of 20m.
2. The spacecraft shall be able to deposit a time capsule of a minimum mass of 2 kg and minimum volume of 2m<sup>3</sup> in the borehole.
3. The spacecraft shall be able to perform in-situ analysis of the retrieved samples.
4. The spacecraft shall be able to retrieve the core samples from the borehole and move them within its body.
5. The spacecraft shall be able to receive new commands and programs from the ground station.

### 5. Reliability and Fault Tolerance Requirements

1. The drill shall have built in redundancy for loss of drill bits.

### 6. Maintenance, Accessibility, Reparability & Testability

1. The drill shall be able to change drill bits autonomously.

### 7. Mandatory Design Safety Factors and Margins

---

1. The spacecraft shall be able to communicate directly with the ground station during the whole descent trajectory.
2. The Spacecraft shall be able to land within a 200mx200m ellipse centred on the target.
3. The spacecraft shall have sufficient data storage to account for an 11.04 day period without Communication.
4. The spacecraft shall have sufficient battery power to last a minimum period of 27.7 hours without power generation.
5. The spacecraft's power generation shall be net positive when under full power load.
6. The spacecraft shall be able to operate on a slope of maximum 15 degrees.

### 8. Cost and Schedule Objectives

1. The spacecraft shall cost no more than 750 FY\$12M, including its launch.
2. The spacecraft shall be ready for launch by the year 2024.

### 9. Performance Definition

1. The spacecraft is able to perform a sample return.
2. The spacecraft is able to fully operate during the night time.
3. The spacecraft is able to operate autonomously throughout communication blackout.
4. The spacecraft is able to characterise the impact history of the landing site [5].
5. The spacecraft is able to assess potential of lunar surface for astronomical observations [5].
6. The spacecraft includes devices used to engage with the public.

## B.3 Work Break down Structure

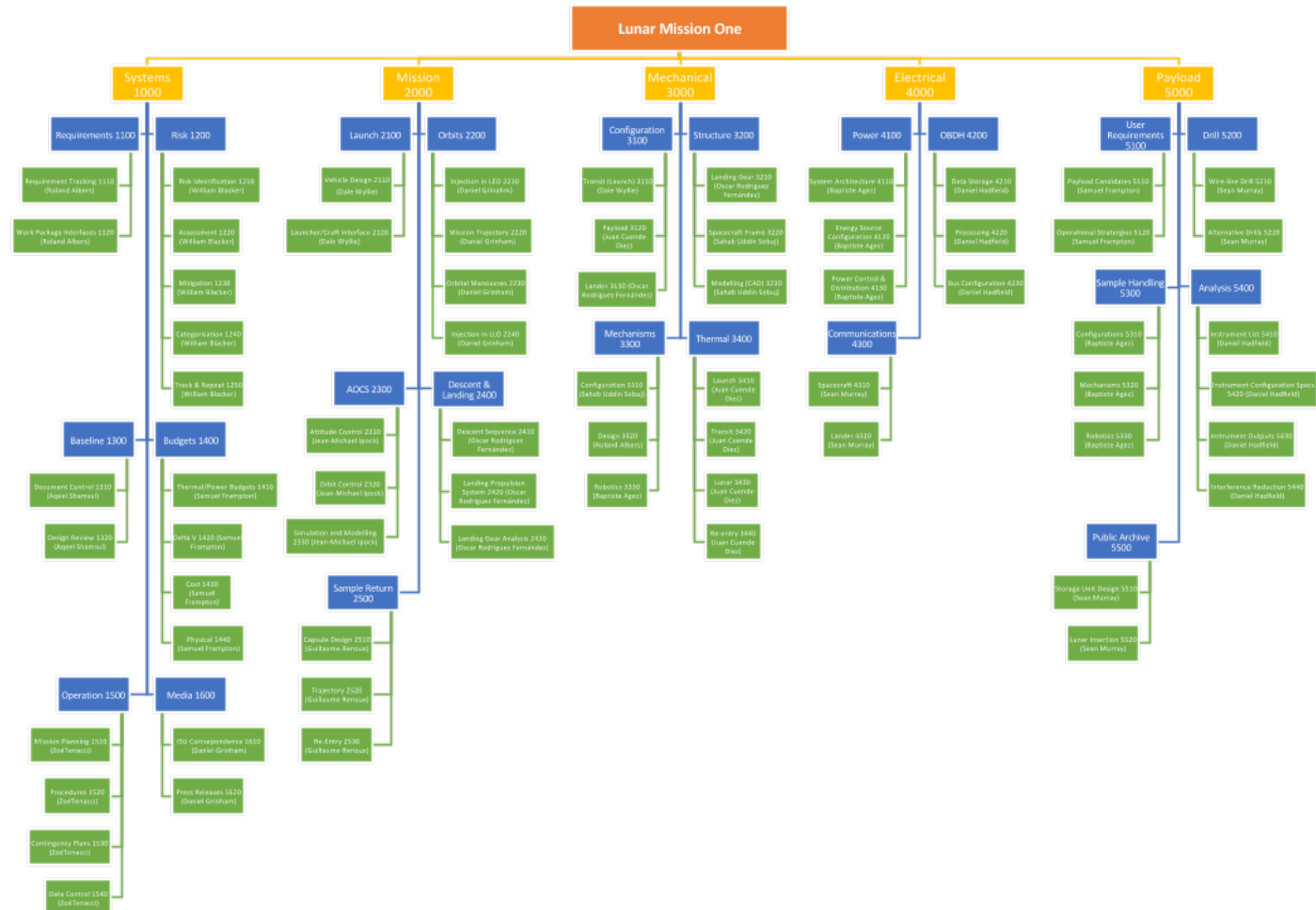
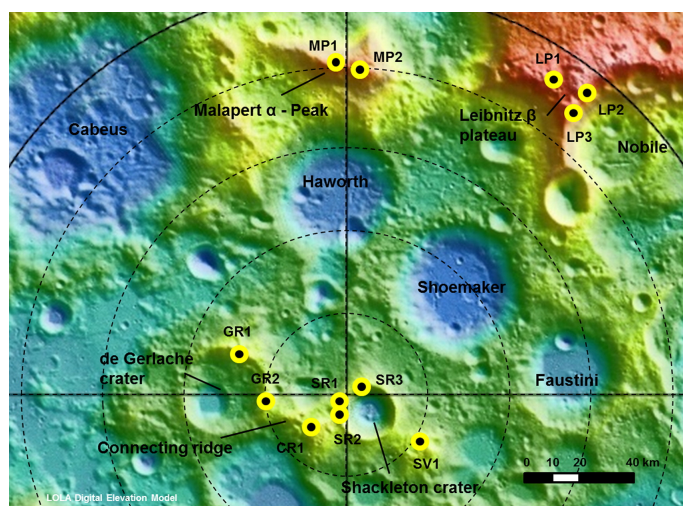


Figure B.1: Chart of Work Breakdown Structure

## B.4 Baseline

This section describes the baseline mission selected by the team to fulfil the requirements and mission statement.

The baseline mission utilises a lander spacecraft to the moon. The chosen landing site is South Pole Atkins next to the Shackleton Crater due to period of illumination and potential volatiles studies. The spacecraft accommodates an automated wireline drill system, 16 scientific instruments and 10 150x40mm public/private archives. The payloads carried were based on the revenue generator for the LM1 project and science goals to understand the properties of lunar environment for the future mankind exploration. Figure B.2 displays the potential landing sites and Figure B.3 represents the CAD model of the spacecraft.



**Figure B.2:** Possible landing sites at the South Pole Atkin near Shackleton Crater labelled SR1, SR2 and SR3 [1]

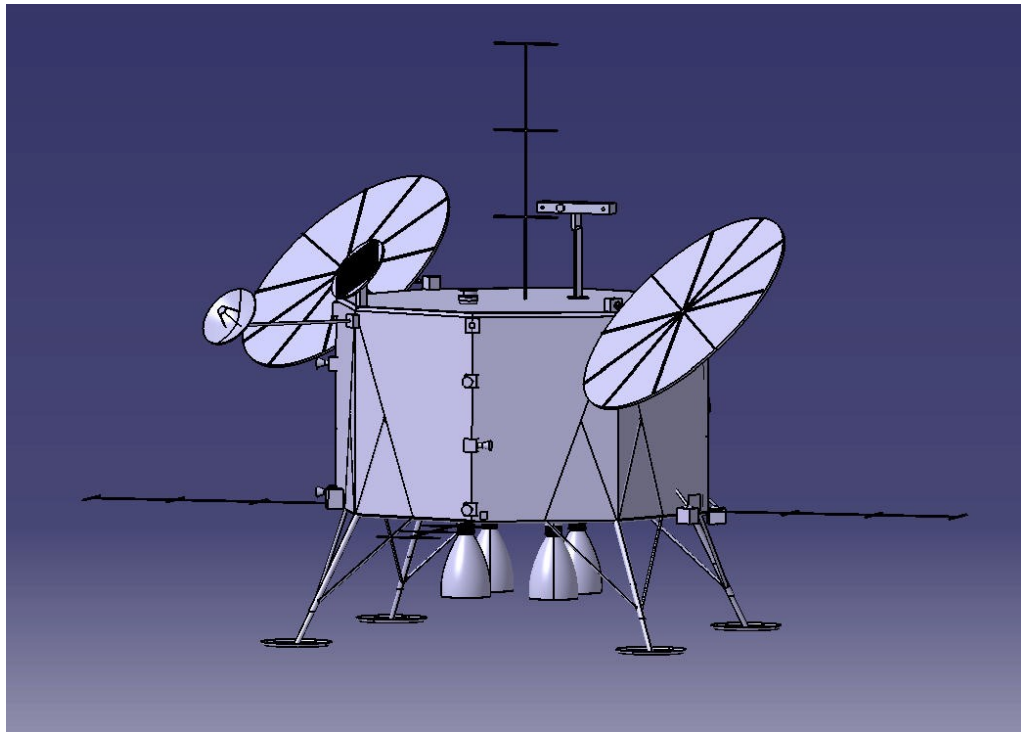


**Figure B.3:** CAD representation of the LM1 Lander

The drill subsystem is the primary component of the spacecraft. It has the capability to drill up to a depth of 100m, retrieving the drilled sample and upon completion deposits the public/private in the borehole. The retrieved sample will be extracted via the borehole to the science payloads for analysis.

Spacecraft Subsystem					
Bill of Materials	Name	Quantity	Mass of module	Dimensions ( mm)	Remark
Propulsion					
2000/01	Main Engine (R-42DM 890 N Dual Mode )	4	35 kg	381 Ø x 635	
2000/02	Thrusters (MONARC-5 engine)	16	9 kg	25 Ø x 418	
2000/03	COPV with PMD Fuel tank	2	50 kg	470 Ø x 1500	Cylindrical tank with spherical end
2000/04	COPV with PMD Oxidiser tank	2	38 kg	402 Ø x 1500	Cylindrical tank with spherical end
2000/05	COPV pressurant tank	2	15 kg	411 Ø x 1500	Spherical tank
2000/06	Tank Structural Mount	1	5 kg		
2000/07	Tank feed system	1	45 kg		
Launch Adapter					
2100/01	Launcher adapter	1	12 kg	3000 Ø x 1000	Attachment for spacecraft to the Falcon 9 fairing
AOCS					
2300/01	Sun sensors	4	1 kg	110 x 110 x 30	
2300/02	Star tracker DPU	2	3 kg	210 x 155 x 56	
2300/03	Star tracker Baffle CHU	2	3 kg	147 Ø x 283	
2300/04	Reaction wheel	4	17 kg	267 Ø x 120	
2300/05	Inertial Measurement Unit LN-200S	1	1 kg	88.9 Ø x 85.1	
Descent and Landing					
2400/01	Flash 3D LIDAR Camera	1	4 kg	120 x 120 x 120	
2400/02	Optical Descent Camera	1	1 kg	70 x 70 x 10	
2400/03	Lidar Altimeter + Velocimeter	1	2 kg	150 x 120 x 150	
2400/04	Mapping Camera	1	1 kg	127 x 122 x 89.2	
2400/05	Inertial Measurement Unit Honeywell	2	11 kg	233 Ø x 169	
Spacecraft Structure					
3200/01	Spacecraft Structure Dry Mass	1	152 kg		Sahab (2016)
Mechanism					
3300/01	Antenna pointing mechanism	2	6 kg		Attached on phased array and TT&C
3300/02	Scalable Rotary actuator	1	4 kg		Mechanism to move the slot underneath the drill
3300/03	Deploying mechanism for seismometer	1	2 kg		Deploying seismometer upon landing
3300/04	Lightweight 2-Axis Mini Gimbal	4	10 kg		Attachment to LIDAR camera. PanCam, phased array (stowing) and TT&C (stowing)
3300/05	Linear actuator	1	9 kg		Deploying mechanism for terrain imager (PanCam)
3300/06	Scalable Rotary actuator	1	2 kg		To allow 360deg rotation for the PanCam
Thermal					
3400/01	Thermal insulation	1	40 kg	N/A	
Power					
4100/01	Li-ion battery VES 180 SAFT	3	33 kg	250 x 106 x 371	
4100/02	Solar Array Triple Junction Cells	1	15 kg	2000Ø	Total weight include both the solar panel and mechanism. The dimension stated is during deployment
4100/03	PCDU Unit	1	17 kg	N/A	Dimensions contain multiple units
OBDH					
4200/01	Flight Computer	1	2 kg	306 x 167 x 30	
4200/02	Mass Memory Unit	2	7 kg	306 x 320 x 60	
4200/03	Space Wire	38	1 kg	N/A	1 unit of space wire is 1m
4200/04	SpW-10X SpaceWire Router	4	0.069 kg	479.4 x 479.4 x 26.5	
4200/05	Remote Terminal Unit µRTU™	5	0.108 kg	70 x 30 x 10	
Communication					
4300/01	Phased Array Antenna	1	20 kg	550 Ø	
4300/02	Parabolic Antenna	1	10 kg	550 Ø x 1232	Attached on a beam
Drill Subsystem					
5200/01	Drill Subsystem	1	83 kg	500 x 500 x 1500	Refer to Appendix B- Drill sub-system component list
5200/02	Regolith Tube	1	2 kg	30 Ø x 500	Made from Boron glass fibre
Sample Handling					
5300/01	Sample Handling Phase 2	1	3 kg	N/A	Dimensions varred on design
5300/02	Sample Handling Phase 3	1	4 kg	N/A	Dimensions varred on design
5300/03	Sample Handling Phase 4	1	4 kg	N/A	Dimensions varred on design
5300/04	Sample Handling Phase 5,6,7	1	4 kg	N/A	Dimensions varred on design
5300/05	Sample Handling Phase 8	1	4 kg	N/A	Dimensions varred on design
Science Payloads					
5400/01	Raman-LIBS Spectrometer	1	2 kg	346 x 317 x 322	
5400/02	Seismometer SES	1	2 kg	440 Ø x 300	
5400/03	Permittivity Probes	2	2 kg	498 Ø x 20	Attached at the landing legs
5400/04	Dust Analyser	1	4 kg	450 x 450 x 600	
5400/05	X-ray Spectrometer	1	1 kg	10 x 115 x 80	
5400/06	Radiation Monitor	1	2 kg	150 x 132 x 68	
5400/07	Radio Astronomy Demonstration Package	5	3 kg	10 x 1000 x 2000	Yagi antenna design
5400/08	Isotope Mass Spectrometer	1	5 kg	250 x 230 x 110	
5400/09	Gamma-Ray Spectrometer	1	3 kg	60 x 60 x 60	
5400/10	Terrain Imager	1	2 kg	300 x 150 x 150	
5400/11	Microscope	1	0.186 kg	40 x 10 x 10	
Public/Private Archive					
5500/01	Archive capsules	10	10 kg	40 Ø x 150	
Instrument Shielding					
6000/01	Spot Shielding for Science Instruments	1	12 kg		Refer to Shamsul (2016) Appendix C - Instruments shielding

Table B.1: Components list

Drill Subsystem					
Bill of Materials	Name	Quantity	Mass of module	Dimensions ( mm )	Remark
<b>Drill Mechanisms</b>					
5200/01/01	Wireline spool	1	13 kg	2.5 Ø x 10500	
5200/01/02	Drilling mechanism	1	33 kg	50 Ø x 1000	
5200/01/03	Drill bits	9	21 kg	50 Ø x 150	
5200/01/04	Drill bits replacement carousal	1	4 kg		
<b>Drill Sample Handling</b>					
5200/01/05	Sampling handling mechanism Phase 1	1	3 kg		
<b>Drill Control Environment</b>					
5200/01/07	Active dust control using electrodynamic dust shield	1	2 kg		Shamsul (2016)
5200/01/08	Bristle Brush	1	2 kg		Taken from similar design for Mars rover
<b>Science Probe</b>					
5400/12	IR Imaging borehole	1	2 kg	25 Ø x 2	
5400/13	Micro-Seismometer	1	0.4 kg	27.6 x 27.6 x 3.6	
5400/14	Borehole Permittivity Probe	1	0.5 kg	27.6 x 27.6 x 3.6	
5400/15	Radiation Monitor	1	0.008 kg	2.54 x 10 x 0.6	
5400/16	Heat Flow Probe	1	0.4 kg	20 Ø x 2	
5400/17	Science probe structure	1	0.6616 kg	50 x 50 x 224	

Table B.2: Drill sub-system components list

Spacecraft Subsystem	Mass
Propulsion	197 kg
Launch adapter	12 kg
AOCS	25 kg
Thermal	40 kg
Power	65 kg
OBDH	11 kg
Communication	30 kg
Drill Subsystem	86 kg
Sample Handling	18 kg
Payloads	27 kg
Public/Private Archive	10 kg
Instruments Shielding	12 kg
Structure	152 kg
Descent and Landing	19 kg
Total Spacecraft Dry Mass	738 kg

Table B.3: Spacecraft sub-system mass

Module	Mass
Spacecraft Dry Mass	738 kg
Extra propellant for contingency	50 kg
Pressurant	7 kg
Total Landing Mass	795 kg

Table B.4: Spacecraft landing mass

Module	Mass
Spacecraft Landing Mass	795 kg
Orbit Trajectories	545 kg
Descent & Landing	663 kg
AOCS Propellant	14 kg
Total Spacecraft Mass	2016 kg

Table B.5: Spacecraft final mass (wet mass)

## B.5 Mission Timeline

For Lunar Mission One, the mission timeline comprises five main mission phases:

- Launch and Early Operations Phase, which includes the launch and the Earth parking orbit the spacecraft will be inserted in [11], [37].
- Lunar transfer, which consists of the spacecraft's journey to the Moon [11].
- Lunar insertion and mapping, which represents the spacecraft's arrival to the Moon and the mapping of the landing site, required for the later landing [11].
- Descent & Landing, which will lead to the spacecraft safely landed on the lunar surface [38].
- On-surface Operations and Science, which includes all the operations to drill beneath the surface and perform sample analysis, i.e. the goal of Lunar Mission One.

Note: For this section, a detailed timeline of all events regarding AOCS has been created by AOCS WP [12]. As it contains numerous events that would overcomplicate the overall timeline and make it unreadable, only key events have been selected to be shown in the Operations timeline. They however have been taken into account, they are only not directly displayed in this Section. More details about this specific timeline can be found in the AOCS report [12].

### B.5.1 Launch and Early Operations Phase (LEOP)

The spacecraft will be launched from Cape Canaveral, Florida (USA) on 28/08/2024 at 12:47 GMT by a Falcon 9 launcher [37]. This date has been chosen by the Orbits and Descent & Landing WPs [11] [38] after the landing date, obtained by Operations WP, has been provided to them.

The launch window is a critical parameter in terms of operations: if the launch window is missed due to weather or technical reasons, the whole orbital trajectory to the Moon will be changed due to the evolution of the relative position of the Earth and the Moon. The Orbits WP has suggested a delay of at least 27 days in order to wait for the same geometrical conditions to be met again [11].

The Launch and Early Operations Phase is designed as follows:

- It will take 10mins for the launcher to place its payload in a circular orbit around the Earth at an altitude of 300km [11].

The payload delivered in this orbit consists of the spacecraft as well as the upper stage of the Falcon 9, still attached to it.

- The payload will stay in parking orbit for 50mins in order to align itself with the trans-lunar trajectory [11].

No health checks will be performed while the spacecraft is in parking orbit.

The spacecraft will stay in stowed configuration and in safe mode (non-essential functions turned off) during the entire duration of the LEOP phase and will rely on its batteries for any power needed.

Two instruments, the dust analyser and the radiation monitor will be turned on and run until the end of the mission [39]. The upper stage of the Falcon 9 will perform any AOCS manoeuvre that may be required as the spacecraft will not have any of its AOCS turned on [12].

- Once it has reached the insertion point in the parking orbit, the upper stage of the Falcon 9 will perform the trans-lunar injection burn on 28/08/2024 at 13:47 [11].

During this manoeuvre, the spacecraft will detach from the upper stage and start its journey to the Moon. The upper stage will remain in Low Earth Orbit (LEO). No controlled re-entry has been planned for it in the scope of this project. In order to comply with ESA's intention to mitigate space debris in LEO, the amount of remaining propellant in the upper stage should be looked at. If enough propellant remain, a de-orbiting burn can be performed in order to make the upper stage reenter the atmosphere and burn.

Event	Starting Date - Duration
1. Launch	28/08/2024 12:47 – 10min
2. Earth parking orbit	28/08/2024 12:57 – 50min
3. Dust analyser and radiation monitor switched on	28/08/2024 12:57 – until end of mission
4. Trans-lunar injection	28/08/2024 13:47

**Table B.6:** Summary of LEO phase

### B.5.2 Lunar transfer

The total duration of the lunar transfer is 2 days 18hrs [11].

- TT&C communications will be turned on on 28/08/2024 at 14:01, i.e. after the spacecraft has started its cruise to the Moon and been detumbled [12]. This will allow health checks of the spacecraft to be performed. TT&C downlink is estimated to last around 10mins.
- On 31/08/2024 at 08:59, the spacecraft will perform an 180deg rotation in order to put the thrusters in the correct orientation for the deceleration that

will be performed to enter the Moon's capture orbit [12]. TT&C communications will once again run in order to check that the spacecraft is in the correct orientation.

Event	Starting Date - Duration
<b>5. Trans-lunar injection</b>	28/08/2024 13 :47
<b>6. Detumbling of S/C</b>	28/08/2024 13 :47 – 13.8min
<b>7. TT&amp;C communications</b>	28/08/2024 14 :01 – 10min
<b>8. Rotation of S/C for thruster alignment</b>	31/08/2024 8 :59 – 13.8min
<b>9. TT&amp;C communications</b>	31/08/2024 11 :13 – 10min

**Table B.7:** Summary of Lunar Transfer Phase

### B.5.3 Lunar insertion and mapping

This phase will last a total of 28 days [11].

- The spacecraft will reach the Moon's vicinity and enter a capture elliptical orbit on 31/08/2024 at 12:00, with a periapsis of 15km altitude in order to perform good lunar surface imaging [11].

TT&C communications will run in order to check that the spacecraft has correctly entered its orbit.

The spacecraft will perform a mapping of the desired landing area and a number of other sites at the South Pole during five orbits, i.e. 8hrs 32min.

- At the end of the mapping sequence, at 19:37, the thrusters will realign themselves in order to reaccelerate the spacecraft into a circular parking orbit of 100km altitude. The spacecraft will stay in this orbit for 27 days 56min in order to wait for the same alignment with the landing site as it was during the mapping phase [11].
- After the spacecraft has reached its circular parking orbit, the data collected during mapping will be downlinked back to Earth for processing. The downlink is estimated to last 10min.
- The data processing is estimated to last 3 days. The updated landing site and sequence will then be uplinked back to the spacecraft on 03/09/2024 at 20:42, which should last about 20min.
- Another thrusters' realignment will take place in order to prepare the spacecraft for its descent and landing sequence [12].
- On 27/09/2024 at 21:28, the spacecraft will enter a landing ellipse and will stay in this orbit for 2hrs 51min before it starts its landing sequence [11].

Event	Starting Date - Duration
<b>10. Elliptical orbit capture</b>	31/08/2024 12 :00
<b>11. Mapping phase</b>	31/08/2024 12:00 – 8hrs 32min
<b>12. S/C detumbling</b>	31/08/2024 12 :00 – 13.8min
<b>13. TT&amp;C communications</b>	31/08/2024 12:14 – 10min
<b>14. Thrusters realignment</b>	31/08/2024 19 :37 – 13.8min
<b>15. TT&amp;C communications</b>	31/08/2024 20 :21 – 10min
<b>16. Circular parking orbit</b>	31/08/2024 20:32 – 27 days 56min
<b>17. Downlink of mapping data</b>	31/08/2024 20:32 – 10min
<b>18. On ground data processing</b>	31/08/2024 20:42 – 3 days
<b>19. Uplink of updated procedures</b>	03/09/2024 20:42 – 20min
<b>20. Thrusters realignment</b>	27/09/2024 19 :03 – 13.8min
<b>21. TT&amp;C communications</b>	27/09/2024 21 :17 – 10min
<b>22. Landing ellipse</b>	327/09/2024 21:28 – 2hrs 51min 56min

**Table B.8:** Summary of Lunar insertion and Mapping Phase

#### B.5.4 Descent and Landing

On 28/09/2024, the spacecraft will start its descent sequence towards the lunar surface that will last a total of 12min [38].

- At 21:28, the spacecraft will go from its circular parking orbit into an elliptical orbit with a periapsis of 15km altitude.
- At 00:19, the spacecraft will reach the periapsis of its orbit and brake for 7min 54s in order to reduce its velocity and altitude.
- Once it has descended down to 4km altitude at 00:27, it will perform an approach phase during 71s.
- At 00:28, at 100m above the lunar surface, the spacecraft will perform a vertical descent for 19s and land at 00:28.

Event	Starting Date - Duration
<b>23. Periapsis brake</b>	28/09/2024 00:19 – 7min 54s
<b>24. Approach phase</b>	28/09/2024 00:27 – 1min 11s
<b>25. Vertical descent</b>	28/09/2024 00:28 – 19s
<b>26. S/C landed</b>	29/09/2024 00:28

**Table B.9:** Summary of Descent and Landing

### B.5.5 On-surface operations and science

On 28/09/2024 at 00:28 the spacecraft will land on the lunar surface and the lunar operations will start. The drilling and sample analysis phase will last a total of 122.34 days.

- The spacecraft will run health checks for 23hrs 32min. TT&C communications will run the entire time.
- On 29/09/2024 at 00:00, the spacecraft will start drilling operations and sample analysis phase.
- On 25/10/2024 at 12:00, the spacecraft will be switched off for 16hrs in order to make it survive the partial solar eclipse encountered on the surface.
- On 26/10/2024 at 04:00, the drilling operations and analysis will start again.
- On 29/01/2025, the drilling and sample analysis phase will be finished and the drill will have reached a depth of 100.8m. The public archives and the science probe will be carried down the borehole and left there.
- The science probe will perform in-situ study of the borehole for as long as possible.
- On 23/02/2025 at 17:45 the spacecraft will be switched off again for 16hrs in order to enable its survivability during the other partial eclipse.
- On 24/02/2025 at 9:45 the spacecraft will be switched on again.
- On 24/03/2025, the landing site will no longer receive enough sunlight to charge its batteries and will then cease to function after a few hours. This will conclude the end of Lunar Mission One.

Event	Starting Date - Duration
<b>27. Health checks</b>	28/09/2024 00:28 – 23hrs 32min
<b>28. Start of drilling operations and sample analysis phase (DOSA)</b>	29/09/2024 00:00 – 27days 12hrs
<b>29. S/C 1st switch off for partial eclipse</b>	25/10/2024 12:00 – 16hrs
<b>30. Continue of DOSA phase</b>	26/10/2024 04:00 – 94 days
<b>31. End of DOSA phase</b>	26/10/2024 04:00 – 94 days
<b>32. Start of extra science phase</b>	29/01/2025 08:10 – 24.74 days
<b>33. S/C 2nd switch off for partial eclipse</b>	23/02/2025 02:00 – 11hrs
<b>34. Continuing of extra science phase</b>	23/02/2025 13:00 – 30 days
<b>35. End of constant illumination period</b>	24/03/2025

**Table B.10:** Summary of on-surface operations and science phase

### B.5.6 Overall timeline of Lunar Mission One

A summary of all the activities performed in the scope of Lunar Mission One can be found [9]. The overall length of the mission, from launch to the loss of optimal illumination conditions is 7 months, which is relatively short for an extra-terrestrial scientific robotic mission.

Events/Phases	Date	Duration
<b>1 - LAUNCH AND EARLY OPERATIONS PHASE</b>		
Launch	28/8/24 12:47	10mins
Earth parking orbit	28/8/24 12:57	50mins
Instruments switch on	28/8/24 12:57	
Trans-lunar injection	28/8/24 13:47	
<b>2 - LUNAR TRANSFER</b>		
TT&C communications	28/8/24 13:57	10mins
Thrusters realignment	31/8/24 8:59	13.8mins
TT&C communications	29/8/24 5:55	10mins
<b>3 - LUNAR INSERTION AND MAPPING</b>		
Elliptical orbit capture	31/8/24 12:00	
TT&C communications	31/8/24 12:00	
Mapping	31/8/24 12:00	8hrs 32min
Thrusters realignment	31/8/24 19:37	13.8mins
Circular parking orbit	31/8/24 20:32	27 days 56min
Downlink of data	31/8/24 20:32	10mins
On ground data analysis	31/8/24 20:42	3 days
Uplink of updated trajectory	3/9/24 20:42	20mins
Thrusters realignment	27/9/24 19:03	13.8mins
Landing ellipse	27/9/24 21:28	2hrs 51mins
<b>4 - DESCENT AND LANDING</b>		
Braking	28/9/24 0:19	9min 52s
Approach phase	28/9/24 0:29	1min 12s
Vertical descent	28/9/24 0:30	17s
S/C landed	28/9/24 0:30	

<b>5 - ON SURFACE OPERATIONS AND SCIENCE</b>		
Health checks	28/9/24 0:30	23hrs 30min
Start of drilling and sample analysis	29/9/24 0:00	27 days 12hrs
S/C 1st switch off for partial eclipse	25/10/24 12:00	16hrs
Continuing of drilling phase	26/10/24 4:00	94 days
End of drilling phase	29/1/25 8:10	
Start of extra science phase	29/1/25 8:10	24,74 days
S/C 2nd switch off for partial eclipse	23/2/25 2:00	11hrs
Continuing of extra science phase	23/2/25 18:00	30 days
End of constant illumination period	24/3/25 0:00	

**Table B.11:** Mission timeline summary

## B.6 Budgets

### B.6.1 Cost Budget

<b>Factor</b>	<b>Cost (FY\$10M)</b>
Spacecraft Bus	106 ± 28
Payload	138 ± 28
Integration, Assembly & Testing	47 ± 19
Program	57 ± 27
Ground Equipment	26 ± 10
Launch	61 ± 12
Insurance	31 ± 6
Software Development	225 ± 45
Operations	63 ± 13
<b>Total</b>	<b>754 ± 188</b>

**Table B.12:** Table of cost

### B.6.2 Power Budget

	<b>Average</b>	<b>Peak</b>	<b>Duration</b>
	<b>W</b>	<b>W</b>	<b>s</b>
<b>Launch Phase</b>	186.22	204.22	686
<b>Parking Orbit</b>	467.38	746.98	3038
<b>Translunar Injection</b>	707.38	986.98	7563
<b>Cruise</b>	491.38	782.98	252725
<b>LOI Burn</b>	707.38	986.98	3465
<b>Moon capture ellipse</b>	491.38	770.98	30716
<b>Burn to circularise</b>	707.38	986.98	91
<b>Moon polar orbit</b>	491.38	770.98	2336180
<b>Burn to landing ellipse</b>	707.38	986.98	91
<b>Landing ellipse</b>	491.38	770.98	10264
<b>Descent and Landing</b>	791.86	1169.86	820
<b>Lunar surface during sunlight</b>	559.18	686.26	17884800
<b>Lunar surface during darkness</b>	81.82	93.82	1662
<b>Margin</b>	1	1	1
<b>Total :</b>	<b>6881.448</b>	<b>9944.928</b>	<b>20532101</b>

**Table B.13:** Power consumption throughout the mission

	<b>Average</b>	<b>Peak</b>
<b>AOCS</b>	116	296
<b>Communications</b>	122	132
<b>Propulsion</b>	180	180
<b>Payload and Sample Handling</b>	75.4	75.4
<b>Structure/Mechanisms</b>	15.4	18.4
<b>OBDH</b>	47.9	67.9
<b>Thermal</b>	80	100
<b>Drill</b>	112	150
<b>Descent and Landing</b>	70.4	106.4
<b>Power</b>	28.18	38.18
<b>Margin</b>	1.2	1.2
<b>Total :</b>	<b>1016.736</b>	<b>1397.136</b>

**Table B.14:** Overall Power Consumption

### B.6.3 $\Delta V$ Budget

Manoeuvre	$\Delta V$ (Km/s)
TLI (launcher)	3.135
LOI	0.903
Circularisation	0.019
Landing ellipse burn	0.019
Descent & Landing	1.939
Total	6.015
<b>Total for S/C</b>	<b>2.88</b>

**Table B.15:** Mission  $\Delta V$  Budget

### B.6.4 Communication

Max power required for TT&C parabolic antenna:	112W	
Max power required with margin (10%):	125W	
Data Rates of both (bps):	2.00E+04	
	10mm thickness	15mm thickness
Mass of one 0.5m diameter, depth 0.06m antenna (Kg):	5.32	7.98
Mass of one 0.5m diameter antenna, depth 0.06m (Kg) with 10% margin:	5.85	8.8
Phased antenna array dimensions:		
Diameter (m):	0.55	
Number of elements:	683	
Transmitter power (w):	12	
Beam Width (deg):	3.6	
Pointing error (deg):	0.36	
X-band (GHz):	8.495	
Data Rate (Mbps):	7.5	
Power limited to (w):	100	
Mass (Kg):	20	
Cost (\$million):	5	
All transmissions and reception done in X - Band (GHz):	8.495	

**Table B.16:** Spacecraft Antennas technical information

<b>Ground Stations:</b>		
<b>New Norcia - DSA1</b>	Australia	North of Perth
Diameter (m):	35	
Transmission waveband:	S - band	X - band
Receiver waveband:	S - band	X - band
Coordinates:	(-31deg 2' 53.61")	(+116deg 11' 29.40")
<b>Cebreros - DSA2</b>	Spain	Madrid
Diameter (m):	35	
Transmission waveband:		X - band
Receiver waveband:	Ku - band	X - band
Coordinates:	(40deg 27' 09.68")	(04deg 22' 03.18")
<b>Malargüe</b>	Argentina	1200km west of Buenos Aires
Diameter (m):	35	
Transmission waveband:		X - band
Receiver waveband:		X - band
Coordinates:	(35deg 46' 33.63")	(69deg 23' 53.51")
<b>Goldstone - DSN</b>	United States	California
Diameter (m):	34	
Transmission waveband:		X - band
Receiver waveband:		X - band
Coordinates:	( <a href="#">35.4267°N</a> )	( <a href="#">116.89°W</a> )

**Table B.17:** Ground Station Details

### B.6.5 Data rates

Instrument	Data Rate (Mbits/s)	Transit Phase (Mbits)	Drilling Phase (Mbits)	Post Drilling Phase (Mbits)	Total with code 70% Inc. (Mbits)
Seismometer	0.001000	0	5,249	4,666	16,856
Permittivity Probes	0.000006	0	31	28	100
Dust Analyser	0.001000	2,678	10,506	4,666	30,345
Radiation Monitor	0.001000	2,678	10,506	4,666	30,345
Radio Astronomy Demonstration Package	0.001000	0	10,506	4,666	25,792
Gamma-Ray Spectrometer	0.016000	0	168,089	74,650	412,656
Terrain Imager	0.016000	0	168,089	74,650	412,656
IR Imaging borehole	2.900244	0	28,453	15,840	75,298
Micro-Seismometer	0.001000	0	5,249	4,666	16,856
Borehole Permittivity Probe	0.000006	0	31	28	100
Micro Radiation Monitor	0.001000	0	5,249	4,666	16,856
Heat Flow Probe	0.000050	0	262	233	842
Raman-LIBS Spectrometer	0.016000	0	1,117	0	1,899
X-ray Spectrometer	0.001000	0	3,492	0	5,936
Isotope Mass Spectrometer	0.000006	0	13	0	22
Microscope	0.012000	0	670	0	1,139
<b>Total With 70% Code Inc.</b>	<b>5.044431</b>	<b>9,105</b>	<b>709,770</b>	<b>328,823</b>	<b>1,047,698</b>

**Table B.18:** Spacecraft Instrument Data rates

## B.7 Configuration

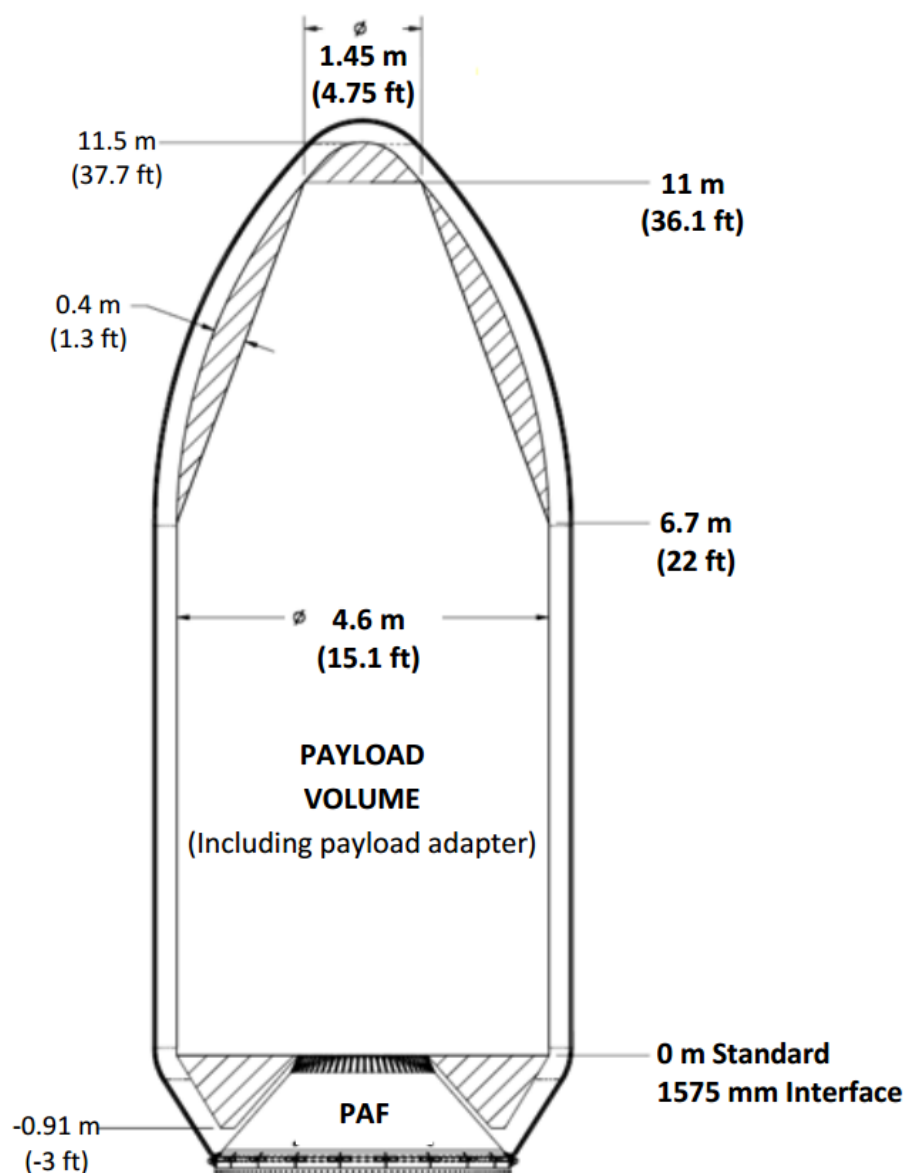


**Figure B.4:** Fairing Dimensions of the Falcon-9 Full Thrust, Space X (2015)

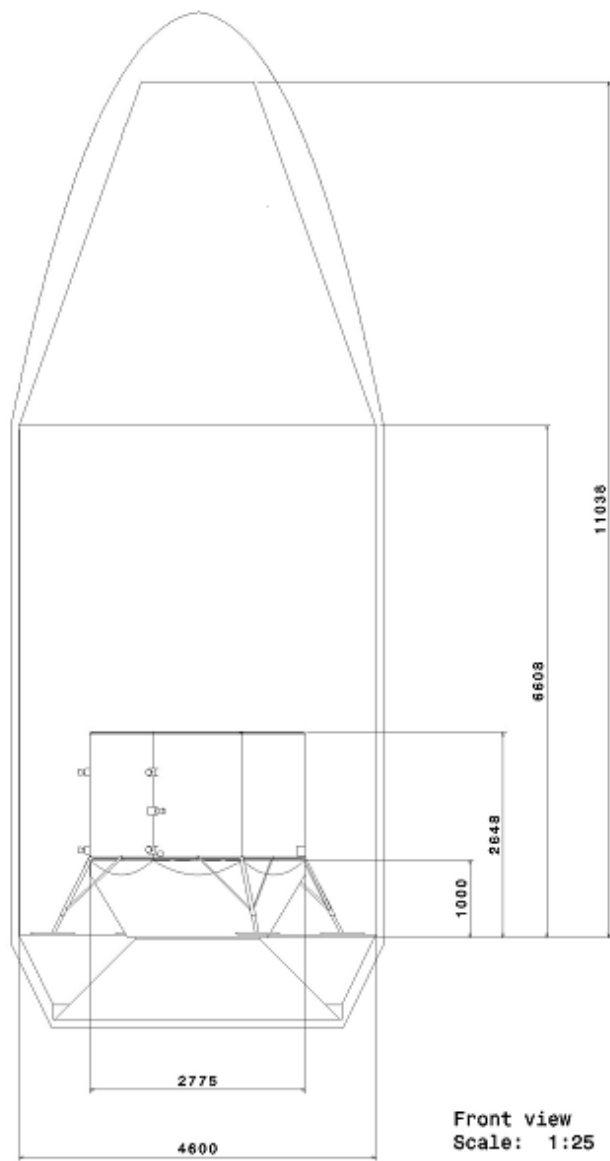


**Figure B.5:** Spacecraft stowed inside the Falcon-9 Full Thrust fairing

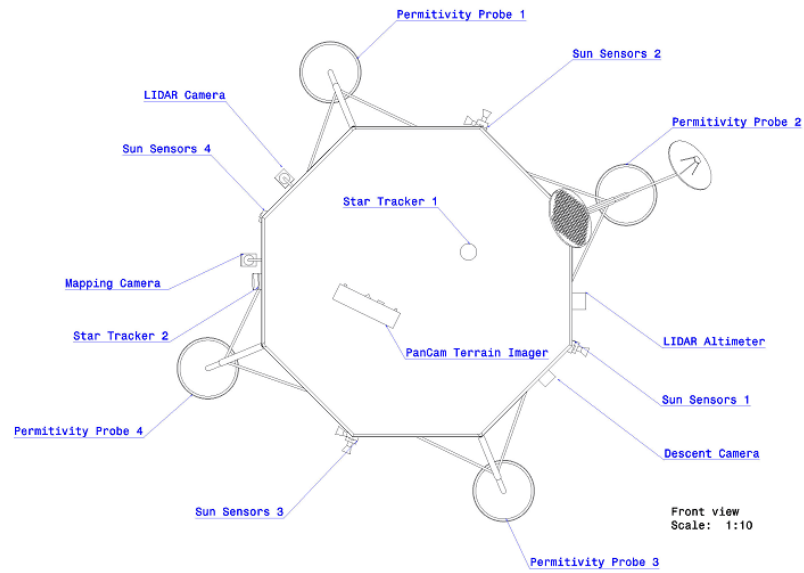


**Figure B.6:** Spacecraft top view

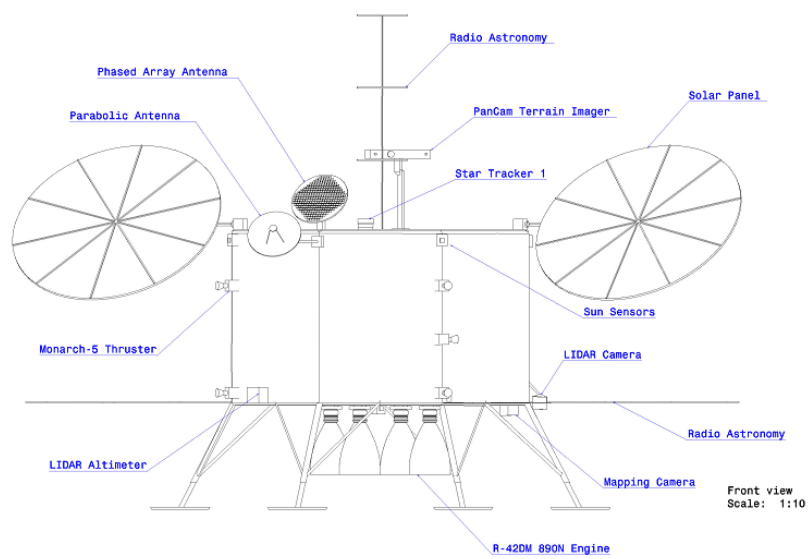


**Figure B.7:** Spacecraft front view

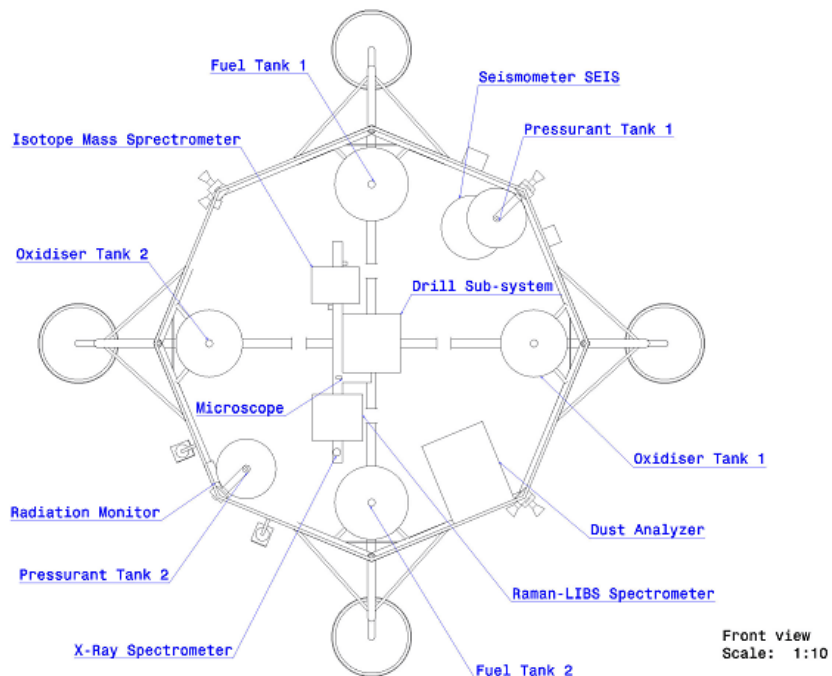


**Figure B.8:** Spacecraft internal view

# Appendix C

## Calculations

In this section some relevant extra calculations are shown for completeness.

### C.1 Preliminary calculation

In this section, preliminary calculations for the descent will be shown.

#### C.1.1 Soft-Landing

From the initial budgets estimations, an initial dry mass of 800 kg will be used.

$$m_{dry} = 800 \quad (\text{C.1})$$

The proposed mission sequence will be as follows:

1. Initial lunar circular polar parking orbit around the Moon with an altitude of 100 km.
2. Transfer into an elliptical orbit with an apoapsis altitude of 100 km and a periapsis altitude of 15 km.
3. A single impulsive burn will kill all the orbital velocity in the periapsis of the elliptical orbit.
4. The spacecraft follows a vertical free fall trajectory.
5. At an altitude of 100 m, the vertical velocity is killed by another impulsive burn and the spacecraft descents at a constant velocity of -1 m/s until touchdown.

Table C.1 sums up the relevant parameters for the soft-landing estimation.

Parameter	Symbol	Value	Units
Dry mass	$m_{dry}$	800	kg
Gravitational Parameter	$\mu_M$	4.9028E12	$\text{m}^3 \cdot \text{s}^{-2}$
Moon Radius	$R_M$	1738200	m
Apoapsis altitude	$h_a$	100000	m
Periapsis altitude	$h_p$	15000	m
Threshold altitude	$h_t$	100	m
Vertical descent velocity	$v_d$	-1	$\text{m} \cdot \text{s}^{-1}$
Engine Specific Impulse	$I_{sp}$	333	s

**Table C.1:** Relevant parameters for the soft-landing calculations

The initial velocity in the circular parking orbit is

$$v_{circular} = \sqrt{\frac{\mu_M}{R_M + h_a}} = 1633 \text{ m} \cdot \text{s}^{-1} \quad (\text{C.2})$$

The velocity in the apoapsis and periapsis of the elliptical orbit is

$$v_{ap} = \sqrt{2\mu_M \left( \frac{1}{R_M + h_a} - \frac{1}{2R_M + h_a + h_p} \right)} = 1613 \text{ m} \cdot \text{s}^{-1} \quad (\text{C.3})$$

$$v_p = \sqrt{2\mu_M \left( \frac{1}{R_M + h_p} - \frac{1}{2R_M + h_a + h_p} \right)} = 1691 \text{ m} \cdot \text{s}^{-1} \quad (\text{C.4})$$

The total velocity achieved during the free fall trajectory is

$$v_{ff} = -\sqrt{2\mu_M \left( \frac{1}{R_M + h_t} - \frac{1}{R_M + h_p} \right)} = -219 \text{ m} \cdot \text{s}^{-1} \quad (\text{C.5})$$

The total  $\Delta v$  for the initial stages is:

$$\Delta V = \Delta V_1 + \Delta V_2 + \Delta V_3 = (v_{circular} - v_{ap}) + (v_p) + (v_d - v_{ff}) \quad (\text{C.6})$$

$$\Delta V = 1929 \text{ m} \cdot \text{s}^{-1} \quad (\text{C.7})$$

For the final constant velocity descent, we can assume that the gravity is constant and equal to the gravity on the Moon surface

$$g_M = \frac{\mu_M}{R_M^2} \quad (\text{C.8})$$

The differential equation that models the dynamics of the constant velocity descent is

$$\frac{d(mV)}{dt} = -mg_M + T \quad (\text{C.9})$$

where  $T$  is the thrust that can be model as

$$T = -\frac{dm}{dt}I_{sp} \quad (\text{C.10})$$

Knowing that

$$v = \frac{dh}{dt} = v_t = -1 \text{ m} \cdot \text{s}^{-1} \quad (\text{C.11})$$

Using C.10 and C.11 in C.9 we obtain:

$$\frac{dm}{m} = \frac{-g_M}{(v_t + I_{sp})v_t} dh \quad (\text{C.12})$$

The integration of C.12 is trivial and gives us a propellant mass for the final constant velocity descent of

$$m_{p_{vd}} = m_{dry} \left( e^{\frac{-g_M h_t}{v_t(v_t + I_{sp})}} - 1 \right) = 40 \text{ kg} \quad (\text{C.13})$$

With this propellant mass and the  $\Delta V$  calculated in C.7, we can use the rocket equation to obtain the total propellant mass required for the descent

$$m_{propellant} = m_{p_{vd}} + (m_{dry} + m_{p_{vd}}) \left( e^{\frac{\Delta V}{I_{sp}}} - 1 \right) \quad (\text{C.14})$$

As a first estimation, the total propellant mass needed for landing is

$$m_{propellant} = 717 \text{ kg} \quad (\text{C.15})$$

### C.1.2 Hard-landing

For a hard landing scenario, the following assumptions will be used:

- Initial lunar circular polar parking orbit around the Moon with an altitude of 100 km.
- Transfer into a elliptical orbit with an apoapsis altitude of 100 km and a periapsis altitude of 0 km.
- The spacecraft is able to dissipate all the kinetic energy of the impact.

The velocity on the circular orbit remains the same:

$$v_{circular} = \sqrt{\frac{\mu_M}{R_M + h_a}} = 1633 \text{ m} \cdot \text{s}^{-1} \quad (\text{C.16})$$

The velocity on the apoapsis of the elliptical orbit is:

$$v_{ap} = \sqrt{2\mu_M \left( \frac{1}{R_M + h_a} - \frac{1}{2R_M + h_a + h_p} \right)} = 1610 \text{ m} \cdot \text{s}^{-1} \quad (\text{C.17})$$

The  $\Delta V$  for this manoeuvre is

$$\Delta V = v_{circular} - v_{ap} = 1633 - 1610 = 23 \text{ m} \cdot \text{s}^{-1} \quad (\text{C.18})$$

The total propellant consumption for this manoeuvre is

$$m_{propellant} = m_{dry} * \left( e^{\frac{\Delta V}{T_{sp}} - 1} \right) = 9.51 \text{ kg} \quad (\text{C.19})$$

The velocity at touch down would be:

$$v_{td} = \sqrt{2\mu_M \left( \frac{1}{R_M} - \frac{1}{2R_M + h_a} \right)} = 1702 \text{ m} \cdot \text{s}^{-1} \quad (\text{C.20})$$

The total kinetic energy that should be dissipated in a hard landing would be:

$$KE = \frac{1}{2}m_{dry}v_{td}^2 = 1159.8 \text{ MJ} \quad (\text{C.21})$$

## C.2 Mapping Camera

Orbit and Viewing Calculations			
Parameter	Value	Unit	Comment
Altitude	15000	m	Periapsis
Period	6828	s	
Ground Track Velocity	1691	$\text{m}\cdot\text{s}^{-1}$	
Node Spacing	1.04	deg	
Moon Angular Radius	82.5	deg	
Elevation Angle	40	deg	Design Parameter
Max Nadir Angle	49.42	deg	
Max Moon Central Angle	0.58	deg	
Max Distance	23195	m	
Swath width	1.16	deg	

**Table C.2:** Orbit and Viewing Calculations for the mapping camera

Pixel Parameters and Data rate			
Parameter	Value	Unit	Comment
Along Track Sampling Distance	3.85	m	Design Parameter
Along Track IFOV	0.00951	deg	
Cross Track Sampling Distance	3.85	m	Design Parameter
Cross Track IFOV	0.00951	deg	
Along Track Ground Pixel Resolution	2.49	m	
Cross Track Ground Pixel Resolution	2.49	m	
Number of Cross Track Pixels	10393		
Number of Along Track Pixels	10393		
Swaths Recorded Along Track in 1 second	439		
Number of Bits to encode each pixel	8	bits	Design Parameter
Number of Spectral Bands	1		Design Parameter
Estimated Data Rate	36.54	Mbps	

**Table C.3:** Pixel Parameters and Data Rate

Sensor Integration Parameters			
Parameter	Value	Unit	Comment
Pixels for Whiskbroom integration	4096		Design Parameter
Swap Width Overlap	1.1		Design Parameter
Pixel Integration Time	0.00035	s	
Pixel Read Out Frequency	2889	Hz	

**Table C.4:** Sensor Integration Parameters

Sensor Optics			
Parameter	Value	Unit	Comment
Cross Track detector size	5.5	$\mu\text{m}$	Design Parameter
Quality Factor for Imaging	1.2		Typical Value
Operating Wavelength	540	nm	Design Parameter
Focal length	331	mm	
Diffraction Limited Aperture	2.7	mm	
F#	9		Design Parameter
Aperture Selected	3.68	mm	Design Parameter
FOV	38.26	deg	
Cut off frequency	$1.52 \cdot 10^5$	$\text{m}^{-1}$	
Nyquist Frequency	$9.09 \cdot 10^4$	$m^{-1}$	
Relative Nyquist Frequency	6		

**Table C.5:** Sensor Optics

Sensor Radiometry			
Parameter	Value	Unit	Comment
Blackbody temperature of Moon	270	K	
Spectral bandwidth	400	nm	Design Parameter
Moon Albedo	0.2		
Average RAdiance	27	$\text{W}\cdot\text{m}^{-2}\cdot\text{sr}^{-1}$	
Radiated power of a single detector	336	$\text{W}\cdot\text{sr}^{-1}$	
Input power at sensor	15.9	pW	
Optical transmission factor	0.8		Typical Value
Input power at detector	12.7	pW	
Available energy	4.41	fJ	
Available photons	1200		
Quatum Efficiency	0.6		Typical Value
Photocarriers available	7180		
Noise electrons	84		
Noise read out electrons	5000		Typical Value
Total noise electrons	71.3		
SNR	101		

**Table C.6:** Sensor Radiometry

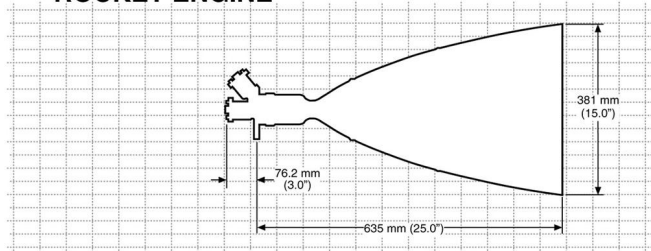
# Appendix D

## Datasheets

### D.1 Aerojet R-42DM

---

#### R-42DM 890 N (200 lbf) DUAL MODE HIGH PERFORMANCE ROCKET ENGINE



#### Design Characteristics

- Propellant ..... Hydrazine / NTO(MON-3)
  - Thrust/Steady State ..... 890 N (200 lbf)
  - Inlet Pressure Range ..... 25.5–13.8 bar (370–200 psia)
  - Chamber Pressure\* ..... 9.6 bar (140 psia)
  - Expansion Ratio ..... 200:1
  - Oxidizer / Fuel Ratio ..... 0.8–1.2 (1.0 nominal)
  - Flow Rate\* ..... 277 g/sec (0.61 lbm/sec)
  - Valve ..... Aerojet Single or Dual Seat
  - Valve Power ..... Various (45 Watts @ 28 Vdc Typical)
  - Mass ..... with single seat valves 7.3 kg (16 lbm)
- \*at rated thrust

#### Performance

- Specific Impulse ..... 327 sec (lbf-sec/lbm)
- Total Impulse .....  $>20.0 \times 10^6$  N-sec ( $4.5 \times 10^6$  lbf-sec)
- Total Pulses ..... >100
- Total Thermal Cycles ..... >50
- Steady State Firing ..... 1000 sec

#### Status

- FY2008 IR&D, TRL 6
- Ready for final flight design and analysis, and formal qualification (program specific)

## D.2 Honeywell Miniature IMU

### MIMU

With more than 40 Miniature Inertial Measurement Units (MIMUs) successfully launched, 120 delivered, and 50 more on order, the MIMU has quickly become the inertial measurement system of choice for commercial and military satellite and space exploration programs.

#### Features

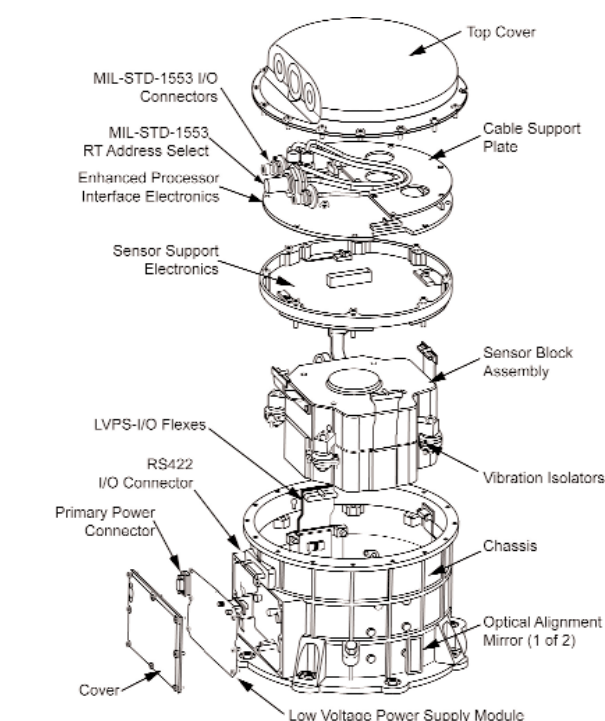
- 3 Axis Angular Measurement using proven GG1320 RLG
- Enhanced Built-in Test
- RS422 and MIL-STD-1553B
- Stimulus Ground Test Function
- Software Upload
- 100 Vdc Primary Power
- In-rush and Current Limiting
- On/Off Command

#### Main Budgets

- Size.....233 mm Ø x 169 mm
- Weight.....≤ 4.7 kg (4.44 Kg Typical)
- Power.....≤ 32 Watts (22 Watts Typical)
- Reliability...≤ 2200 FIT (30°C)

#### Performance (Typical)

- Range...± 375 deg/sec
- Bias (1σ)...≤ 0.005 deg/hr
- ARW (1σ)...≤ 0.005 deg/rt-hr
- Scale Factor (1σ)...≤ 1 ppm



#### Environments

- IA Alignment (1σ)...≤ 1.70μrad
- Pyrotechnic Shock 40,000g
- -30°C to 65°C (operating)
- Radiation Hardened
- Space Vacuum
- -100 Krad Total Dose
- EMI per MIL-STD-461c
- - SEU Tolerant
- Acceleration 25g
- - Latchup Immune
- Random Vibration 19.7 grms
- Available Options

- Primary Power 28Vdc to 100 Vdc
- Velocity Channel

#### Find out more

For more information regarding the MIMU, contact us at:  
<http://www.honeywell.com/sites/aero/Space.htm>

#### Honeywell

Defense & Space  
 13350 US Highway 19 North  
 Clearwater, Florida 33764-7290  
 Tel: 602.365.3099  
[www.honeywell.com](http://www.honeywell.com)

DFOISR# 03-S-1918  
 G61-0401-000-000  
 January 2006  
 © 2006 Honeywell International Inc

**Honeywell**

## D.3 Northrop Grumman LN-200S IMU



**T**he LN-200S inertial fiber-optic gyro for space applications offers outstanding accel/gyro bias and random walk performance.

### Description

The LN-200S is a small, lightweight, highly reliable, state-of-the-art fiber-optic inertial measurement unit (IMU). The LN-200S comprises three solid-state fiber-optic gyros and three solid-state silicon Micro Electro-Mechanical Systems accelerometers in a compact package that measures velocity and angle changes in a coordinate system fixed relative to its case. Digital output data of incremental velocity and angle are provided to user equipment over a digital serial data bus.

The LN-200S has the performance of the LN-200 family, with additional screening and utilization of radiation-tolerant components for space environments. Additionally,

the LN-200S has the same form factor as the standard LN-200.

The LN-200S can be installed with software variations that include selectable data rate outputs from delta thetas and delta velocities.

### Applications

Designed for short- to medium-term space missions, the LN-200S provides highly reliable attitude reference and acceleration data for moderate performance demands, including:

- Earth and heliocentric orbits
- Missions lasting up to six years
- Moderate three-axis inertial reference

### Advantages

Adapted from Northrop Grumman's medium accuracy IMU, the LN-200S maintains performance, even in demanding environmental conditions. The unit is hermetically

sealed, which is advantageous for planetary and asteroid probes. The non-dithered, low-voltage inertial sensors ensure long, reliable usage life and low noise. The LN-200S IMU has been utilized and is still performing on the NASA Mars rovers after more than 10 years. The LN-200S has the lowest gyro and accelerometer white noise in the medium accuracy IMU class.

With full IMU functionality, the LN-200S performs critical functions in a spacecraft attitude control system. Its wide dynamic range makes it ideal for attitude determination and high maneuvers such as spacecraft slewing, despinning and thrust measurements. Its accelerometers provide inertial data useful for delta-V and other specific force measurements.

**Heritage**

The LN-200S is part of the LN-200 product line, which has been in high-rate production since 1994 with more than 25,000 units produced. Northrop Grumman has a broad, strong business base for this family of systems and can ensure its availability and support for even the most demanding production quantities. Benefiting from the production line, the low-cost LN-200S unit is highly attractive to missions for flight demonstration, sensor redundancy and multiple phases.

The first prototype LN-200S was qualified for space flight onboard the Clementine spacecraft. Many spacecraft now depend on the IMU to provide reliable inertial data for low-earth orbit and space probe missions. Additional spacecraft that use the LN-200S include the following:

- BATSSAT (Teledesic I)
- Deep Space I
- TSX-5
- MightySat II
- Space Station Interim Control Module
- Shuttle/SAFER
- VCL
- OrbView-3
- GRACE
- QuikTOMS
- Muses-C
- Coriolis
- Mars Rover (Spirit, Opportunity, and now, Curiosity)

Performance	
Accelerometer (1σ)	
Bias Repeatability	300 µg, 1σ
Noise	35 µg/√Hz
Scale Factor Accuracy	300 ppm, 1σ
Input Axis Alignment	0.1 mrad
Max Input Accel	40 g
Gyro (10σ)	
Bias Repeatability	1°/hr, 1σ
Bias Stability (60 min)	<0.1°/hr
Scale Factor Stability	100 ppm
Angle Random Walk	<0.07°/√hr
Input Axis Alignment	0.1 mrad
Dynamic Range (max)	1,000°/sec
Bandwidth	200 Hz @ 400 Hz data rate

Characteristics	
Power	12w nominal, regulated at ±5 Vdc and ±15 Vdc
Dimensions	Diameter: 3.5 in. (8.89 cm) Height: 3.35 in. (8.51 cm) (plus connector)
Weight	1.65 lb (748 g)
Volume	35 in³
Temperature Range	-54°C (-65.2°F) to +71°C (+159.8°F)
Survival Temp Range	-62°C (-79.6°F) to 85°C (+185°F) Perf
Shock	400 g/100 Hz; 1,500 g/1,000 Hz
Vibration (survival)	15 g rms random
Radiation Tolerant	10 Krad
Electrical Interface Protocol	RS-422/485 serial data
Enclosure	Hermetically sealed

**For more information, please contact:**

Northrop Grumman  
Navigation and Maritime Systems  
21240 Burbank Boulevard  
Woodland Hills, CA 91367 USA  
1-866-NGNAVSYS (646-2879)  
[www.northropgrumman.com](http://www.northropgrumman.com)

[www.northropgrumman.com](http://www.northropgrumman.com)

© 2013 Northrop Grumman Systems Corporation  
All rights reserved.  
25441\_022013



DS-474-JYC-0213  
ePROCS: 13-0452  
2013 WH Graphics

**THE VALUE OF PERFORMANCE.**

**NORTHROP GRUMMAN**

## D.4 Efacec Lidar Velocimeter/Altimeter



### Overview

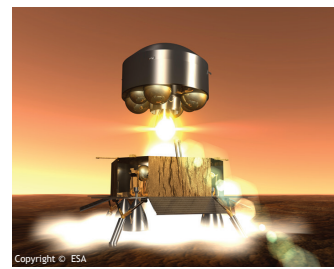
A direct and reliable measurement of the ground distance by a terrain sensor is a key asset for any planetary descent and landing system that allows the triggering of key events of the entry, descent and landing sequence (EDL).

Depending on the environment LIDAR or RADAR versions may be preferred options, or a combined solution using both versions with technology redundancy.

Several missions are targets for these Altimeters:

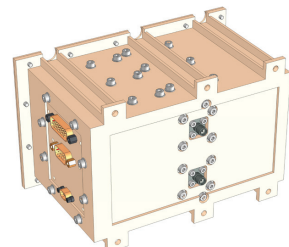
- Mars landing missions
- Moons landing missions
- Asteroids landing missions

Efacec development focuses on low resources European Altimeters able to meet the stringent requirements of those missions.



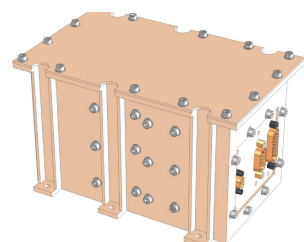
### Benefits

- Low mass
- Low power
- Low communication link budget
- Integrated algorithms
- Updatable configuration during cruise phase



### Functionalities

- Measure distance from 7km down to 10m
- Accuracy of  $0,33\% \pm 0,8m$
- Calculate distance, speed and acceleration
- Kalman filter built-in
- Communicate through Space-Wire / CAN-Bus
- Powered by spacecraft 28V rail
- HV-HPC On/Off Command
- BSM On/Off Status
- BSM single trigger configurable alarm

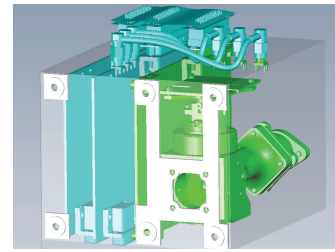


Altimeter Flight model



**Technical Characteristics****Functional Characteristics**

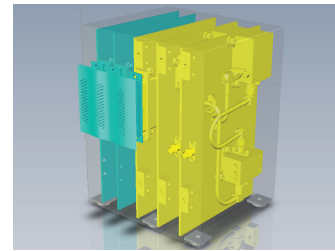
- Powered by 28V DC
- Communicates using the Space-Wire or CAN-bus
- ON/OFF HV-HPC commands
- ON/OFF BSM Status
- Configurable distance trigger alarm - BSM
- Discrete telemetry
- EGSE port for (re)calibration purposes
- Reports time tagged distance (1ms accuracy) and derivate data upon host request
- Housekeeping information reporting instrument health-check @ 1min resolution
- RADAR / LIDAR frontend disable functionality to allow in-flight verification / validation / SW update



LIDAR Altimeter - Breadboard model

**Typical Specifications**

- |                                    |                                 |
|------------------------------------|---------------------------------|
| • Power consumption                | 6W                              |
| • Weight                           | 1.5kg                           |
| • Size                             | 150 x 120 x 150 mm <sup>3</sup> |
| • Field of View                    | 10°                             |
| • Measurement rate                 | 20Hz (RADAR) or 10Hz (LIDAR)    |
| • Fulfils the following standards: |                                 |
| ◦ ECSS                             |                                 |
| ◦ ESCC                             |                                 |
| ◦ Space-Wire                       |                                 |
| ◦ CAN-Bus                          |                                 |
| ◦ MIL-STD-883                      |                                 |



RADAR Altimeter - Breadboard model



Efacec Electric Mobility, S.A.

Rua Eng. Frederico Ulrich - Ap. 3078 | 4471-907 Moreira Maia | Portugal | Phone: +351 229 402 000 | Fax: +351 229 485 428 | e-mail: aerospace@efacec.com | web: www.efacec.com



Due to continuous development, specifications may change without notice. Not valid as a contractual element.

## D.5 DragonEye Flash Lidar 3D Camera

### ASC 3DFLCs for OOS Applications STS Flight Qualified 3DFLC

Quantities Measured:	Range and Intensity
Detectors:	128 x 128 ROIC/ InGaAs APD array.
Performance:	1 meter (5 cm precision) to 4 km (60 cm precision).
Optical/Mechanical Design:	12 mm aperture f/1.6 telescope, aluminum construction.
Field of View:	45 by 45°
In-Flight Calibration:	Single time of flight optical reference.
Mounting Orientation:	Fixed to spacecraft.
Thermal Requirements:	Operating -10° C to +40° C. Storage -20° C to +60° C.
Frame Rate:	20 Hz
On-board Data Processing:	Virtex 4 FPGA
Mass:	3 kg
Size:	12 x 12 x 12 cm
Power:	30 W 100% duty cycle (28 -32 Vdc)



As Flown  
Configuration  
7/15/09



Approved for public release, distribution unlimited.



[www.asc3d.com](http://www.asc3d.com)